Redox Biology 82 (2025) 103594

Contents lists available at ScienceDirect

Redox Biology

journal homepage: www.elsevier.com/locate/redox

Interleukin-35 inhibits NETs to ameliorate Th17/Treg immune imbalance during the exacerbation of cigarette smoke exposed-asthma via gp130/STAT3/ferroptosis axis

Peizhi Tao [1], Beiting Su [1], Xueyan Mao [1], Yusen Lin, Li Zheng, Xiaoling Zou, Hailing Yang, Jing Liu [*], Hongtao Li [**]

Department of Pulmonary and Critical Care Medicine, The Third Affiliated Hospital of Sun Yat-sen University, Institute of Respiratory Diseases of Sun Yat-sen University, Guangzhou, People's Republic of China

ARTICLE INFO

Keywords:
Interleukin-35
Neutrophil extracellular traps
Th17 cell
Treg cell
Cigarette smoke exposed-asthma

ABSTRACT

Cigarette smoke (CS) exposure amplifies neutrophil accumulation. IL-35, a novel cytokine with anti-inflammatory properties, is involved in protection against asthma. However, the biological roles of neutrophils and the precise molecular mechanisms of IL-35 in CS exposed-asthma remain unclear. We showed that the exacerbation of CS exposed-asthma leads to dramatically increased neutrophil counts and an imbalance in DC-Th17/Treg immune responses. RNA sequencing revealed that NETs, part of a key biological process in neutrophils, were significantly upregulated in the context of CS exposed-asthma exacerbation and that IL-35 treatment downregulated NET-associated gene expression. Targeted degradation of NETs, rather than neutrophil depletion, alleviated the CS exposed-asthma. Mechanistically, STAT3 phosphorylation promoted ferroptosis, exacerbating NET release, which in turn enhanced dendritic cell (DC) antigen presentation, activated T cells, and specifically promoted Th17 cell differentiation while inhibiting Treg cells. IL-35 acting on the gp130 receptor alleviated STAT3-mediated ferroptosis-associated NET formation. In summary, our study revealed a novel mechanism by which IL-35 inhibited NET formation, subsequently alleviating neutrophilic inflammation and restoring the DC-Th17/Treg imbalance in CS exposed-asthma, highlighting the potential of IL-35 as a targeted therapeutic strategy.

1. Introduction

Asthma is a heterogeneous chronic respiratory condition that affects approximately 300 million individuals globally [1]. The Global Burden of Disease (GBD) 2015 study estimated that asthma contributed to 1.1 % of global disability-adjusted life years (DALYs), imposing significant healthcare and economic burdens [2]. A subsequent GBD 2017 analysis further emphasized the ongoing public health challenge, reporting that chronic respiratory diseases, including asthma, affected 544.9 million people worldwide [3]. Cigarette smoke (CS) is a significant environmental risk factor for asthma exacerbation [4,5], contributing to an increased frequency of acute episodes, reduced corticosteroid efficacy, and impaired symptom control in affected individuals [6]. Regarding smoking-related asthma cases, active smoking is associated with a 1.89-fold increased risk of asthma with airflow limitation in adults [7]. Furthermore, passive smoking exacerbates asthma severity, particularly in children, as demonstrated by a 18.2 % annual reduction in pediatric asthma hospitalizations after smoke-free legislation in Scotland [8]. Globally, secondhand smoke exposure contributed to 36,900 asthma-related deaths annually, emphasizing its role in asthma morbidity [9]. More importantly, smoking scars the immune system (especially adaptive immunity) for years even after quitting [10]. CS triggers an abnormal immune response, characterized by elevated levels of circulating neutrophils, macrophages, T lymphocytes, and other immune cells. Our previous studies demonstrated that Th2/Th17 polarization is linked to inflammation in CS exposed-asthma models [11,12]. Th17/Treg imbalance also play a critical role in the pathogenesis of asthma; however, the mechanisms driving Th17/Treg imbalance in the

* Corresponding author.
** Corresponding author.
E-mail addresses: liuj779@mail2.sysu.edu.cn (J. Liu), lihongt2@mail.sysu.edu.cn (H. Li).
[1] These authors are equal contributions to the article.

https://doi.org/10.1016/j.redox.2025.103594
Received 11 February 2025; Received in revised form 12 March 2025; Accepted 12 March 2025
Available online 12 March 2025

context of CS exposure remain unclear.

Neutrophils are the first innate immune cells infiltrating the airways in response to CS exposure [13,14]. The use of neutrophil extracellular traps (NETs) is a novel antimicrobial strategy employed by neutrophils. These are three-dimensional, filamentous extracellular structures decorated with granule-derived proteins [15]. Recent studies reveal that NETosis-derived extracellular dsDNA correlates with airway symptoms during viral-triggered asthma exacerbations, establishing a mechanistic link between NET formation and asthma progression [16]. In several chronic respiratory diseases, persistent neutrophil influx and continuous NET release obstruct the airways, leading to impaired lung function [17]. Chronic pulmonary infections have also been linked to the presence of large amounts of neutrophil proteins and DNA in sputum, which are believed to originate from NETs [18]. Currently, multiple publications have reported that increased levels of NETs are linked to asthma [19,20], although the exact nature of this relationship remains poorly understood.

IL-35, a recently discovered inhibitory cytokine composed of an α chain (p35 subunit) and a β chain (Epstein-Barr virus-induced gene 3, EBi3), is a member of the IL-12 family [21]. Recent studies have underscored the importance of IL-35 in various pathological conditions, including cancer and autoimmune diseases. In the context of allergic asthma, the overexpression of IL-35 has been shown to significantly reduce the levels of neutrophils, eosinophils, Th17 cells, and inflammatory cytokines (IL-4, IL-5, IL-13, and IL-17A) in bronchoalveolar lavage fluid (BALF), alleviate airway hyperresponsiveness (AHR), and diminish airway inflammation [22,23]. Furthermore, IL-35 has been reported to mitigate allergic inflammation by inhibiting the activation and accumulation of inflammatory lymphocytes at sites of inflammation [24]. Notably, a 2023 study demonstrated that recombinant IL-35-BCG therapy inhibited neutrophil recruitment and restored immune imbalance through JNK pathway modulation in neonatal asthma models, suggesting its potential for early-life interventions in environmentally exacerbated asthma [22]. Our previous study preliminarily suggested that IL-35, in conjunction with DCs, inhibits Th2 and Th17 cell differentiation and drives Th1/Treg cell responses [11]. However, the molecular mechanisms by which it regulates innate and adaptive immunity require further investigation.

Critically, although emerging studies established the association between NETs and asthma pathogenesis, the following critical gaps remain unaddressed in the context of cigarette smoke exposure: (a) whether CS acts synergistically with asthma to amplify NET formation, thereby disrupting DC-mediated Th17/Treg homeostasis; (b) given IL-35's established role in restraining asthmatic airway inflammation, does it functionally interact with key NET-associated modalities; (c) what are the precise molecular circuits through which IL-35 governs NET dynamics; (d) can therapeutic IL-35 delivery counteract the CS-induced "NET-immune vicious cycle" to reverse neutrophilic inflammation in CS exposed-asthma.

In this study, we focused on the immunoregulatory effects of NETs on DC-mediated T-cell differentiation and the role of IL-35 in targeting NETs in CS exposed-asthma. We demonstrated that IL-35, which is dependent on neutrophil gp130 receptors, interacts with STAT3 to influence ferroptosis-associated NETs, thereby alleviating the DC-Th17/Treg imbalance and neutrophilic inflammation. These results highlight the significant therapeutic potential of IL-35 for alleviating airway inflammation in patients with CS exposed-asthma.

2. Methods

Detailed descriptions of the methods are provided in the supplementary material.

2.1. Cigarette smoke exposed-asthma murine model

Female C57BL/6J mice aged 6 to 8 weeks were purchased from GemPharmatech Co. All animal protocols were approved by the Institutional Animal Care and Use Committee of Jennio Biotech Co., Ltd (No. JENNIO-IACUC-2023-A015). The animals were maintained in a controlled, specific pathogen-free environment with a 12-h light-dark cycle and access to standard rodent chow and water.

The model mice with CS exposed-asthma were divided into four groups: control group, CS group, house dust mite (HDM) group and HDM combined with cigarette smoke (HDM/CS) group (n = 6/group). The models were generated as previously described [11] with minor modifications. Briefly, the HDM group and HDM/CS group were sensitized via intraperitoneal (i.p.) administration of 20 μg HDM (XPB82D3A2.5, Greer Laboratories) in conjunction with 66.7 μL alum adjuvant (77161, ThermoFisher Scientific) dissolved in 133.3 μL of PBS on Days 0 and 14, after which the mice were subjected to intranasal (i.n.) inhalation challenges with 10 μg HDM in 20 μL PBS thrice weekly for 5 weeks. For the CS exposure regimen, the CS group and HDM/CS group were subjected to the inhalation of smoke from 10 unfiltered cigarettes for approximately 30 min twice daily for 5 d per week during the HDM challenge period. The mice in the control and HDM groups were exposed to ambient room air.

2.2. Drug intervention in vivo

In some experiments, the mice were intraperitoneally injected with deoxyribonuclease I (DNase I; 10 mg/kg/mouse; DN25, Sigma-Aldrich) [25], IL-35 (400 ng/mouse, 200-37, PeproTech) [24], SC144 (gp130 inhibitor; 10 mg/kg; HY-15614, MCE) [26], colivelin TFA (STAT3 activator, 1 mg/kg; C912884, Macklin) [27], or saline 0.5 h before HDM challenge until the termination of the experiment, with dosages chosen in accordance with previous studies.

2.3. Neutrophil depletion

Neutrophil depletion was conducted as previously described with minor modifications [28,29]. Two hundred micrograms of anti-Ly6G antibody (BE0075, Bio X Cell) or rat IgG2a isotype control antibody (BE0089, BioXCell) were delivered by i.p. administration twice weekly for 5 weeks during the challenge period until the termination of the experiment.

2.4. Cell culture, differentiation and treatment

The differentiated HL-60 neutrophil-like (dHL-60) cells represent a well-characterized and widely accepted model for studying NETs *in vitro* [30]. The human acute promyelocytic leukemia cell line (HL-60; MeisenCTCC, China) was suspended in HL-60 specific culture medium (CM-0110, Pricella) in 5 % CO_2 at 37°C. HL-60 cells were differentiated into neutrophil-like cells by culture in medium supplemented with 1.25 % v/v DMSO (0219605580, MP) for 7 d. The level of dHL-60 cells was assessed by flow cytometry analysis of CD11b (301305, BioLegend) expression [31]. To establish a drug intervention-based CS exposed-asthma model, human peripheral blood neutrophils (PBNs) or dHL-60 cells (1×10^6) were pretreated with or without rhIL-35 (0-100 ng/mL; CHI-HF-21035, AdipoGen) [32], Cl-amidine (100 μM; HY-100574A, MCE) [33], or Fer-1 (1 μmol/L; A4371, APExBIO) [34] for 30 min, followed by stimulation with HDM (0.5 μg/mL Der p1, XPB91D3A25, Greer Laboratories) [35] and 0.2 % CSE for 24 h.

2.5. Gene silencing or overexpression

The gp130 siRNA and the corresponding scrambled control were purchased from TranSheep Bio (Shanghai, China). The sense sequence for gp130 siRNA was "5′–CCAGUCCAGAUAUUUCACAUUdTdT–3′". The scrambled sequence was "5′–UUCUCCGAACGUGUCACGUTT–3′". STAT3 overexpression (OE-STAT3) was achieved by transfection of the pCDH-MSCV-STAT3 vector (TranSheep Bio, China) with Lipofectamine 3000

(TL301-01, Vazyme) according to the manufacturer's protocol. The cells were collected after 48 h of transfection for further study.

2.6. ELISA

The human serum concentrations of IL-35 (MM-1683H1, Meimian), IL-17A (MM-2117H1, Meimian), MPO-DNA (MM-2467H1, Meimian), HMGB-1 (MM-1623H1, Meimian), and NE (E-EL-H1946, Elabscience) were measured using ELISA kits in accordance with the manufacturers' instructions.

2.7. Western blot

Cells or murine lung tissues were lysed with RIPA lysis buffer (HB504A, HUAYUN) supplemented with a proteinase inhibitor (HYY187, HUAYUN). Protein samples were separated by the SDS-PAGE (PG212, Epizyme) and then transferred onto a PVDF membrane (ISEQ00010, Merck Millipore). After blocking with 5 % nonfat milk (232100, BD) or 5 % BSA (180728, MP), the membranes were incubated with primary antibodies, including anti-STAT3 (1:2000; 8204S, CST), anti-p-STAT3 (1:2000; 8204S, CST), anti-gp130 (1:1000; 3732S, CST), anti-citrullinated histone H3 (Cit-H3; 1:1000; ab5103, Abcam), anti-GPX4 (1:2000; T56959, Abmart), anti-transferrin receptor 1 (TFR1; 1:500; T56618, Abmart), anti-β-actin (1:1000; R1102-1, HUABIO), and anti-GAPDH (1:5000; ET1601-4, HUABIO), at 4 °C overnight followed by incubation with an HRP-conjugated secondary antibody.

2.8. Ferroptosis quantification

Lipid peroxidation, a hallmark of ferroptosis [36], was assessed by measuring malondialdehyde (MDA) levels using an MDA assay kit (HYZ410, HUAYUN), according to the manufacturer's instructions. The oxidized glutathione (GSSG) and total glutathione (T-GSH) levels were estimated using a Total GSH/GSSG Colorimetric Assay Kit (E-BC-K097-S, Elabscience). The levels of 4-HNE (4-Hydroxynonenal) were measured using 4-HNE ELISA Kit (E-EL-0128c, Elabscience).

2.9. Scanning electron microscopy (SEM)

Stimulated neutrophils were fixed at 4°C for 24 h in 2.5 % glutaraldehyde. Following routine dehydration and sputter coating procedures, NET structures were examined using a scanning electron microscope (Hitachi, SU8100) operated at an acceleration voltage of 3.0 kV.

2.10. Statistical analysis

The data are presented as the means ± standard errors of the means (SEMs). Statistical significance was determined using a two-tailed Student's *t*-test or one-way ANOVA followed by the Newman-Keuls post hoc test for multiple comparisons, as appropriate. Pearson's correlation or Spearman's rank correlation was used to assess the relationships between variables in the clinical sample, based on the distribution of the data. $P<0.05$ was considered statistically significant. All statistical analyses were performed using GraphPad Prism version 9.0 (GraphPad Software, Inc., La Jolla, CA, USA).

3. Results

3.1. A neutrophil-driven phenotype contributed to the exacerbation of CS exposed-asthma in a murine model

To determine the pathophysiological mechanism underlying CS exposed-asthma exacerbation, we established a murine model of CS exposed-asthma in the presence of HDM-induced airway disease (Fig. 1A). Initially, methacholine challenge tests were carried out to examine the AHR. As shown in Fig. 1B, compared with control mice, mice with CS exposed-asthma showed a dramatic worsening of AHR. Subsequently, pathological changes in the lung tissues were examined. As shown in Fig. 1C, the HDM/CS group exhibited severe cell infiltration, mucus secretion, and collagen accumulation. Notably, we documented significantly increased numbers of neutrophils and mild increases in eosinophil counts in both the lungs and BALF of mice in the HDM/CS group (Fig. 1D-F). Further immunological analysis revealed increased expression of the costimulatory molecules CD40 and CD86 on DCs from both the lungs and spleen of mice in the HDM/CS group (Fig. 1G and H). Similarly, compared to the control mice, the proportion of Th17 cells was significantly greater in both the lungs and spleen, whereas the Treg cell count was markedly lower in the spleen (Fig. 1I-L). These results indicate that CS exposure exacerbates the neutrophilic inflammation and DC-Th17/Treg imbalance in CS exposed-asthma model mice, closely resembling neutrophilic asthma in humans.

3.2. Neutrophil depletion failed to have a protective effect

Given that neutrophils may play a critical role in CS exposed-asthma, we wondered whether neutrophil depletion via anti-Ly6G antibody (or IgG2a isotype control) could improve airway inflammation (Fig. 2A). As anticipated, anti-Ly6G antibody treatment effectively reduced the number of neutrophils in both the BALF and the lungs of mice. Interestingly, however, the proportion of eosinophils unexpectedly increased in the anti-Ly6G group compared with the IgG2a isotype control group (Fig. 2B and C), suggesting that neutrophil depletion may lead to a compensatory increase in eosinophils. Pathologically, although the inflammatory parameters such as the proportions of neutrophils and eosinophils differed between the anti-Ly6G and IgG2a isotype control groups, the overall degree of inflammation, mucus secretion, and airway remodeling were similar (Fig. 2D). With respect to immune cell profiles, neutrophil depletion did not significantly reduce CD40 and CD86 expression on DCs in the lung or spleen (Fig. 2E-G). Additionally, the Th17/Treg imbalance was not substantially reversed in either organ (Fig. 2H-K). In summary, these data imply that indiscriminate blockade of overall neutrophil function might not always be beneficial in the context of CS exposed-asthma exacerbation.

3.3. Increased NET release in the CS exposed-asthma model

These interesting results prompted us to perform whole-transcriptome sequencing of mouse lung tissues to further explore the function of neutrophils in the pathophysiology of CS exposed-asthma. The principal component analysis (PCA) results are depicted in Fig. S3, which illustrates the distribution and variance of the dataset. As shown in Fig. 3A and Table S3, compared with the control, 2357 genes were identified as differentially expressed genes (DEGs), including 1681 upregulated genes and 676 downregulated genes. The GO pathway analysis of the DEGs revealed that "immune-related function" was markedly enriched (Fig. 3B), and the KEGG pathway analysis further revealed that the "neutrophil extracellular trap formation pathway", a critical biological function related to activated neutrophils, was significantly enriched (Fig. 3C). Furthermore, genes associated with neutrophil extracellular trap formation (pathway id: mmu04613) presented increased expression in the HDM/CS group, as indicated by the heatmap (Fig. 3D) and GSEA results (Fig. 3E). Therefore, we decided to focus on identifying crosstalk between NETs and disease exacerbation.

To assess NET formation in the context of CS exposed-asthma, we quantified NETs in the lungs using Western blot and immunofluorescence staining. Compared with that in the control group, the number of NETs (Fig. 4A and B) was significantly greater in the HDM/CS group. Additionally, we utilized fresh neutrophils isolated from the peripheral blood of healthy donors, along with dHL-60 cells, as *in vitro* study subjects, which were cultured and stimulated with HDM/CS to mimic CS exposed-asthma. The level of HL-60 cell differentiation and purity of the

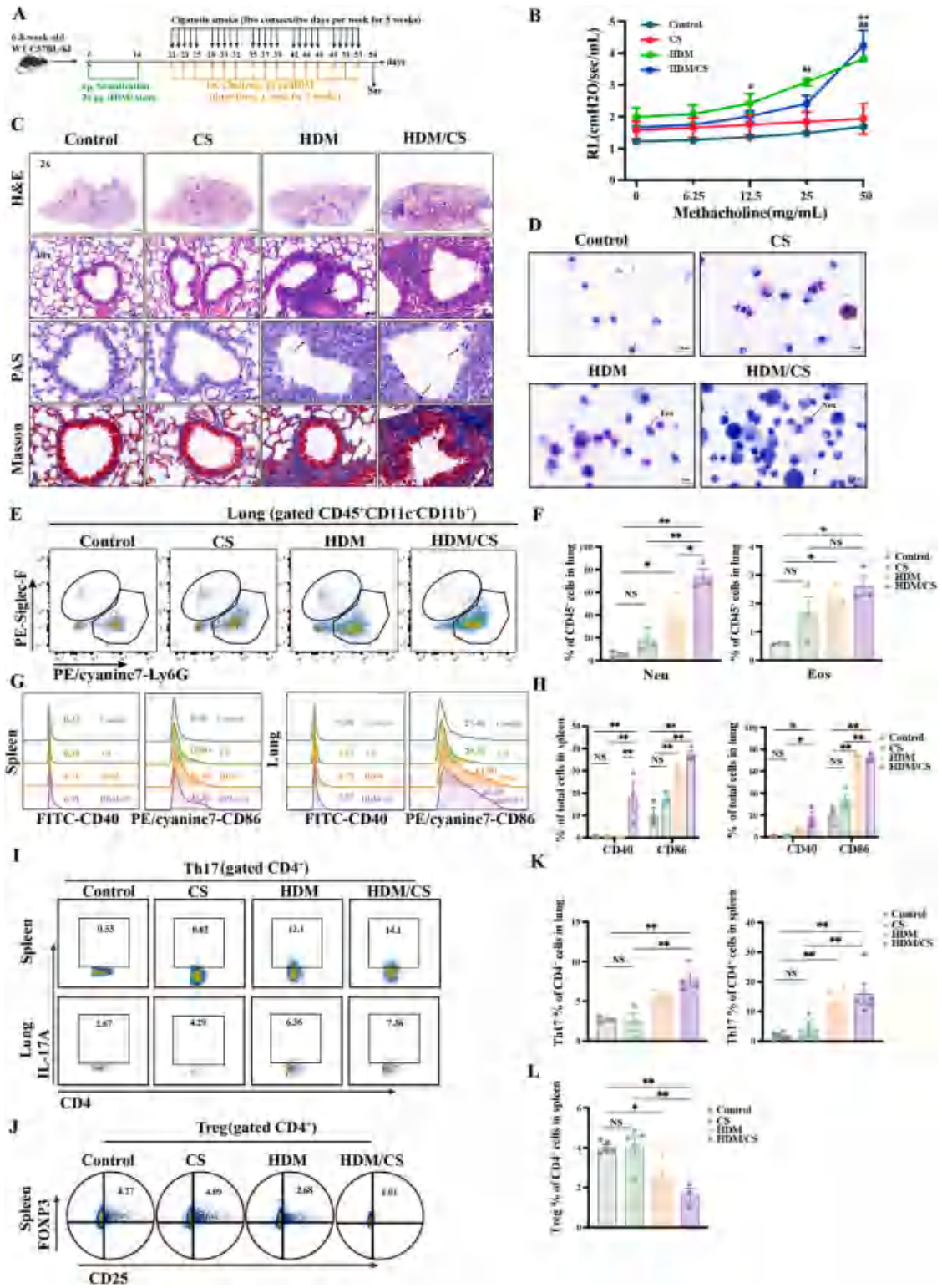

Fig. 1. Neutrophil-driven phenotype in the CS exposed-asthma murine model. (A) Experimental timeline for CS exposed-asthma murine model. (B) Lung resistance (R_L) measured in response to increasing concentrations of methacholine (0, 6.5, 12.5, 25, and 50 mg/mL) (* HDM/CS *vs* Control; # HDM *vs* Control). (C) Representative images of histologic mice lung sections stained with H&E (scale bars, 1 mm for 2x magnification and 40 μm for 40x magnification, arrow: typical areas), PAS (scale bars, 40 μm, arrow: typical areas), and Masson (scale bars, 40 μm, arrow: typical areas). (D) Diff-quick staining of BALF (scale bars, 20 μm). (E) Eosinophils ($CD45^+CD11^-CD11b^+SiglecF^+$) and neutrophils ($CD45^+CD11^-CD11b^+Ly6G^+$) in the lungs of mice were analyzed by flow cytometry. (F) Quantification of neutrophils and eosinophils from panel (E). (G) Matured DCs ($CD45^+CD11c^+CD40^+$ and $CD45^+CD11c^+CD86^+$ cells) in the lungs and spleens of mice were analyzed by flow cytometry. (H) Quantification of CD40 and CD86 expression from panel (G). (I) Th17 ($CD4^+IL\text{-}17A^+$) cells in the lungs and spleens of mice were analyzed by flow cytometry. (J) Treg ($CD4^+CD25^+Foxp3^+$) cells in the spleens of mice were analyzed by flow cytometry. (K and L) Quantification of Th17 cells and Treg cells from panel (I) and (J). Data represent mean with SEM. $^*P < 0.05$; $^{**}P < 0.01$.

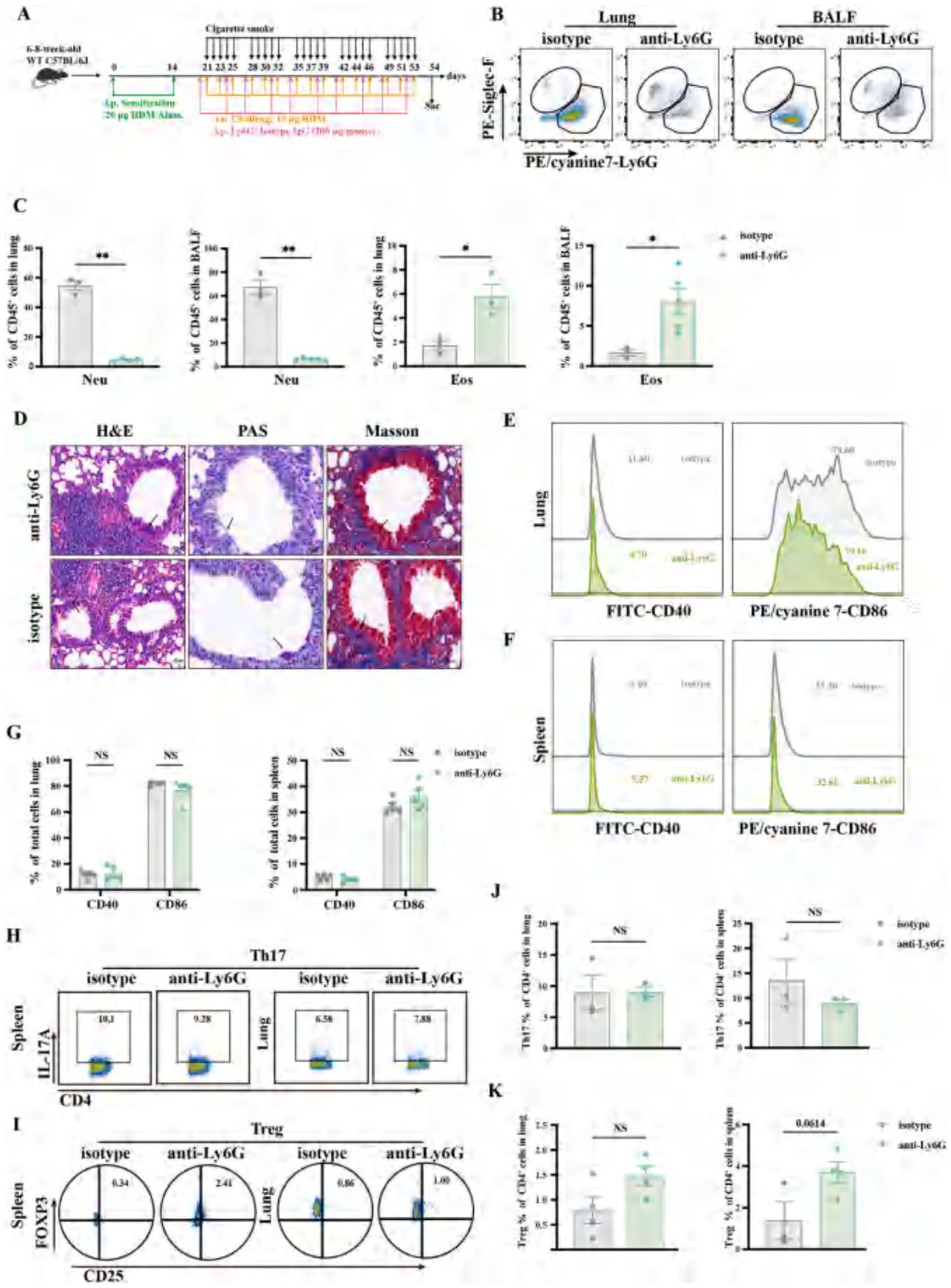

Fig. 2. Neutrophil depletion showed no significant protective effect on CS exposed-asthma exacerbation. (A) Anti-Ly6G was injected intraperitoneally at 24 h before HDM challenge to deplete neutrophils as the time shaft indicated. Rat IgG2a isotype was used as a control. (B) Eosinophils ($CD45^+CD11^-CD11b^+SiglecF^+$) and neutrophils ($CD45^+CD11^-CD11b^+Ly6G^+$) in the lungs and BALF of mice were analyzed by flow cytometry. (C) Quantification of neutrophils and eosinophils from panel (B). (D) Representative images of histologic mice lung sections stained with H&E, PAS, and Masson (scale bars, 40 μm, arrow: typical areas). (E and F) Matured DCs ($CD45^+CD11c^+CD40^+$ and $CD45^+CD11c^+CD86^+$ cells) in the lungs and spleens of mice were analyzed by flow cytometry. (G) Quantification of CD40 and CD86 expression from panel (E) and (F). (H and I) Th17 ($CD4^+IL\text{-}17A^+$) and Treg ($CD4^+CD25^+Foxp3^+$) cells in the lungs and spleens of mice were analyzed by flow cytometry. (J and K) Quantification of Th17 cells and Treg cells from panel (H) and (I). Data represent mean with SEM. $^*P < 0.05$; $^{**}P < 0.01$.

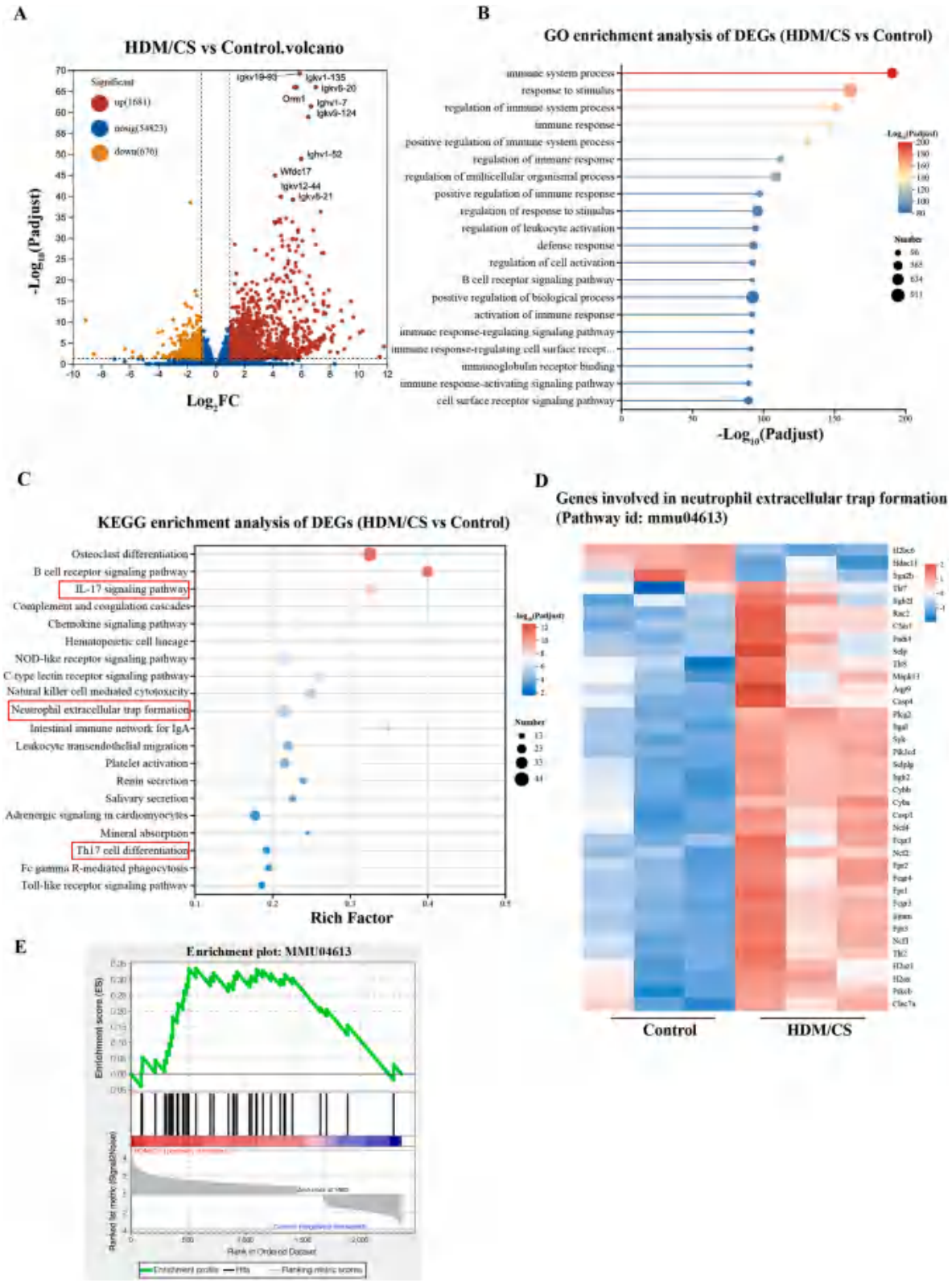

Fig. 3. RNA sequencing revealed that neutrophil-related function in HDM/CS group mice. (A) Volcano plot of DEGs in HDM/CS *vs* control mice. Upregulated genes are shown in red, while downregulated genes are shown in yellow-brown, with a $\log_2$ (fold-change)| >1 and $P < 0.05$. (B and C) The DEGs based on fold change in HDM/CS *vs* control mice were analyzed for GO pathway and KEGG pathway analysis. (D and E) The genes related to the NET formation pathway, which is a defined pathway in KEGG pathways (id: mmu04613), were selected and displayed in heatmap (D) and GSEA analysis (E).

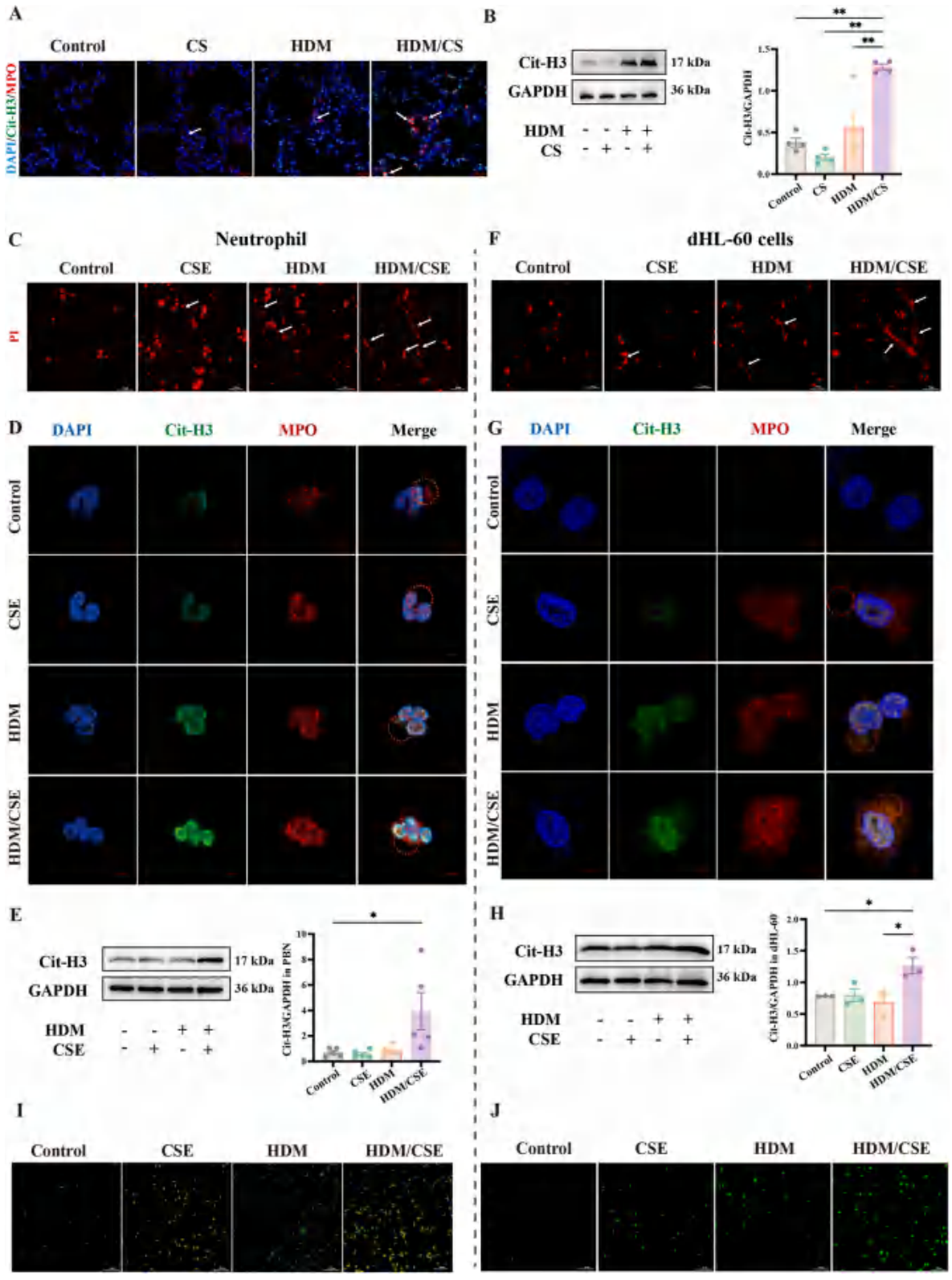

Fig. 4. NETs were significantly increased both *in vivo* and *in vitro*. (A) Lung tissues were subjected to immunofluorescence staining with Cit-H3 (green), MPO (red), and DAPI (blue) to detect NET formation (NETs: white arrows, scale bars, 10 μm). (B) Western blot analysis of Cit-H3 protein levels in mouse lung tissue, quantified using Image J. (C and F) Immunofluorescence images of PI staining of dsDNA in neutrophils (C) and dHL-60 cells (F) (NETs: white arrows, scale bars, 50 μm). (D and G) Representative immunofluorescence staining of Cit-H3 (green), MPO (red), and DAPI (blue) to visualize NET formation in neutrophils (D) and dHL-60 cells (G) detected by confocal laser scanning microscopy (Red circle: NETs, scale bars, 50 μm). (E and H) Protein levels of Cit-H3 in neutrophils (E) and dHL-60 cells (H) were measured by Western blot and analyzed by Image J. (I and J) DCFH-DA staining to detect redox stress levels both in neutrophils (I) and dHL-60 cells (J) (scale bars, 50 μm). Data represent mean with SEM. $^{*}P < 0.05$; $^{**}P < 0.01$.

neutrophils were assessed, as shown in Fig. S4. Consistent with the *in vivo* results, we observed a marked increase in dsDNA release and the colocalization of Cit-H3 and MPO, alongside elevated Cit-H3 protein levels in both human PBNs (Fig. 4C-E) and dHL-60 cells (Fig. 4F-H) treated with HDM combined with cigarette smoke extract (HDM/CSE).

Given that NET formation is closely linked to oxidative stress, we further assessed redox stress using DCFH-DA staining. As expected, redox stress levels were significantly elevated in both PBNs and dHL-60 cells upon HDM/CSE stimulation (Fig. 4I and J). In conclusion, these findings indicate that the extensive formation of NETs in individuals with CS exposed-asthma may contribute to the exacerbation and progression of the disease.

3.4. Beneficial effects of NET removal on airway inflammation and T-cell modulation

We next investigated whether removal of NETs could alleviate airway inflammation exacerbated by CS exposure. DNase I, which has been shown to degrade NETs by cleaving cell-free DNA, is proposed to have therapeutic potential [37]. Therefore, we administered DNase I to the mice prior to each challenge (Fig. 5A). Treatment with DNase I resulted in a reduction in AHR (Fig. 5B). In line with this functional improvement, histological analysis revealed a marked decrease in peribronchial and perivascular inflammatory cell infiltration, goblet cell hyperplasia, and collagen deposition (Fig. 5C). In parallel, flow cytometry analysis revealed that DNase I treatment significantly suppressed the expression of CD40 and CD86 on DCs (Fig. 5D-F). Moreover, DNase I treatment decreased the proportion of Th17 cells and increased the proportion of Treg cells (Fig. 5G-J), suggesting that NETs may serve as initial triggers of immunopathology.

We hypothesized that NETs act as "linchpins" linking the innate and adaptive immune responses *in vitro*. To test this hypothesis, we used HDM/CSE-induced NETs to simulate DCs and then cocultured them with naïve $CD4^+$ T cells, using PMA-induced NETs as positive controls (Fig. 6A). DCs (Fig. S5) and naïve $CD4^+$ T cells (Fig. 6B) were prepared from the peripheral blood mononuclear cells (PBMCs) of healthy donors. As anticipated, DCs exposed to NETs presented elevated levels of CD40 and CD86 (Fig. 6C), indicating that NETs directly enhance the antigen presentation capacity of DCs, which is crucial for DC-mediated T-cell differentiation. In terms of antigen-specific T-cell responses, compared with those cocultured with untreated DCs, naïve $CD4^+$ T cells cocultured with NET-pretreated DCs generated fewer $CD4^+CD25^+CD127^-$ Treg cells (Fig. 6D) and a greater percentage of $CD4^+IL\text{-}17A^+$ Th17 cells (Fig. 6E). Taken together, these findings suggest that NETs play a key role in activating DCs and T-cell differentiation, whereas neutrophils play a paradoxical role in this process.

3.5. RNA sequencing revealed the underlying mechanisms by which IL-35 alleviates CS exposed-asthma exacerbation

Although the removal of NETs has beneficial effects on alleviating airway inflammation and modulating T-cell responses, the lack of pharmacologically safe and effective agents for NET degradation limits its clinical application. Building on our initial findings of the therapeutic potential of IL-35 in regulating immune functions in individuals with CS exposed-asthma [11], we further investigated its molecular mechanisms with an emphasis on key immune pathways and cellular interactions. We performed RNA-seq analysis of lung tissue from mice with CS exposed-asthma both with and without IL-35 treatment. The PCA results are presented in Fig. S6. In total, 1533 DEGs were identified in the lung tissue from both the HDM/CS/IL-35 and HDM/CS groups, comprising 407 upregulated genes and 1126 downregulated genes (Fig. 7A and Table S4). IL-35 treatment predominantly modulated immune-related pathways, including "immune system process", "regulation of immune system process", and "immune response-regulating signaling pathway" (Fig. 7B). KEGG analysis (Fig. 7C) revealed IL-35-induced suppression of the NET formation pathway (KEGG Pathway ID: mmu04613), with corresponding downregulation of neutrophil extracellular trap-related genes confirmed by heatmap analysis (Fig. 7D).

We further performed WGCNA to identify potential gene modules associated with HDM and CS exposure, as well as with IL-35 treatment, and identified six distinct modules (Figs. S7A and B). We observed that a unique gene module (MEblue) was activated in the HDM/CS group but suppressed in the other groups. GO (Fig. S8A) and KEGG (Fig. S8B) analyses of the 1535 genes (Table S5) identified in the MEblue module revealed significant enrichment in pathways related to "immune response, the IL-17 signaling pathway, and neutrophil extracellular trap formation". These findings highlight the potential of IL-35 in regulating immune responses, particularly NET formation, in CS exposed-asthma exacerbation.

3.6. IL-35 protected against CS exposed-asthma exacerbation in mice through inhibiting NET formation

To further elucidate the biological effect of IL-35, we administered recombinant IL-35 during the challenge period (Fig. S9). We observed markedly reduced expression of the IL-35 subunits EBi3 and P35 in HDM/CS group mice (Fig. 8A). Compared with HDM/CS group, IL-35 treatment alleviated AHR (Fig. 8B) and pathological damage (Fig. 8C). To explore the immune-modulatory role of IL-35 in greater depth, we conducted a thorough analysis of immune cell dynamics. Flow cytometry revealed a marked reduction in neutrophil infiltration within the lungs following IL-35 treatment (Fig. 8D and E). In addition, IL-35 treatment led to a substantial downregulation of CD40 and CD86 expression on DCs (Fig. 8F and G). These changes were accompanied by a significant decrease in Th17 cell populations and a concurrent increase in Treg cells (Fig. 8H-L). These findings collectively suggest that IL-35 exerts a potent regulatory effect on immune responses, balancing innate and adaptive immunity in the context of CS exposed-asthma.

With respect to NET formation, we observed reduced Cit-H3 protein levels (Fig. 8M) and decreased lung colocalization of Cit-H3 and MPO (Fig. 8N) under IL-35 treatment, providing strong evidence that IL-35 downregulates NET formation to alleviate neutrophil-driven inflammation and restore the DC-Th17/Treg imbalance.

3.7. IL-35 directly inhibited NET formation through the STAT3/ferroptosis axis in vitro

To further investigate the ability and molecular mechanisms of IL-35 in regulating NETs *in vitro*, we assessed NET formation in neutrophils and dHL-60 cells stimulated with HDM/CSE and incubated with varying concentrations of IL-35 (0, 50, and 100 ng/mL). We observed that treatment with 100 ng/mL IL-35 led to a significant reduction in NET formation, as evidenced by a marked decrease in dsDNA release detected by PI (Fig. 9A and B) and quantified using a NanoDrop One (Fig. S10). Further analysis revealed a substantial decrease in the colocalization of Cit-H3 and MPO (Fig. 9C and D), accompanied by reduced levels of Cit-H3 protein following IL-35 treatment (Fig. 9E and F). SEM provided additional validation, showing that IL-35 similarly suppressed NET structure in PBNs (Fig. 9G). In summary, these results confirmed the significant ability of IL-35 to inhibit NET formation. Moreover, IL-35 treatment significantly reduced ROS production in response to HDM/CSE stimulation (Fig. S11), highlighting its potential to mitigate neutrophil-driven inflammation and prevent subsequent tissue damage.

Both NET formation and ferroptosis are linked to similar intracellular signaling pathways in the progression of certain diseases [34,38]. In this context, we found that ferroptosis was significantly elevated in the CS exposed-asthma model, as evidenced by increased levels of TFR1, MDA, and 4-HNE, along with a marked decrease in GPX4 expression. Additionally, GSH metabolism analysis revealed a significant increase in Oxidized Glutathione (GSSG) levels and a decrease in Total Glutathione (T-GSH), GSH and GSH/GSSG ratio further confirming ferroptosis

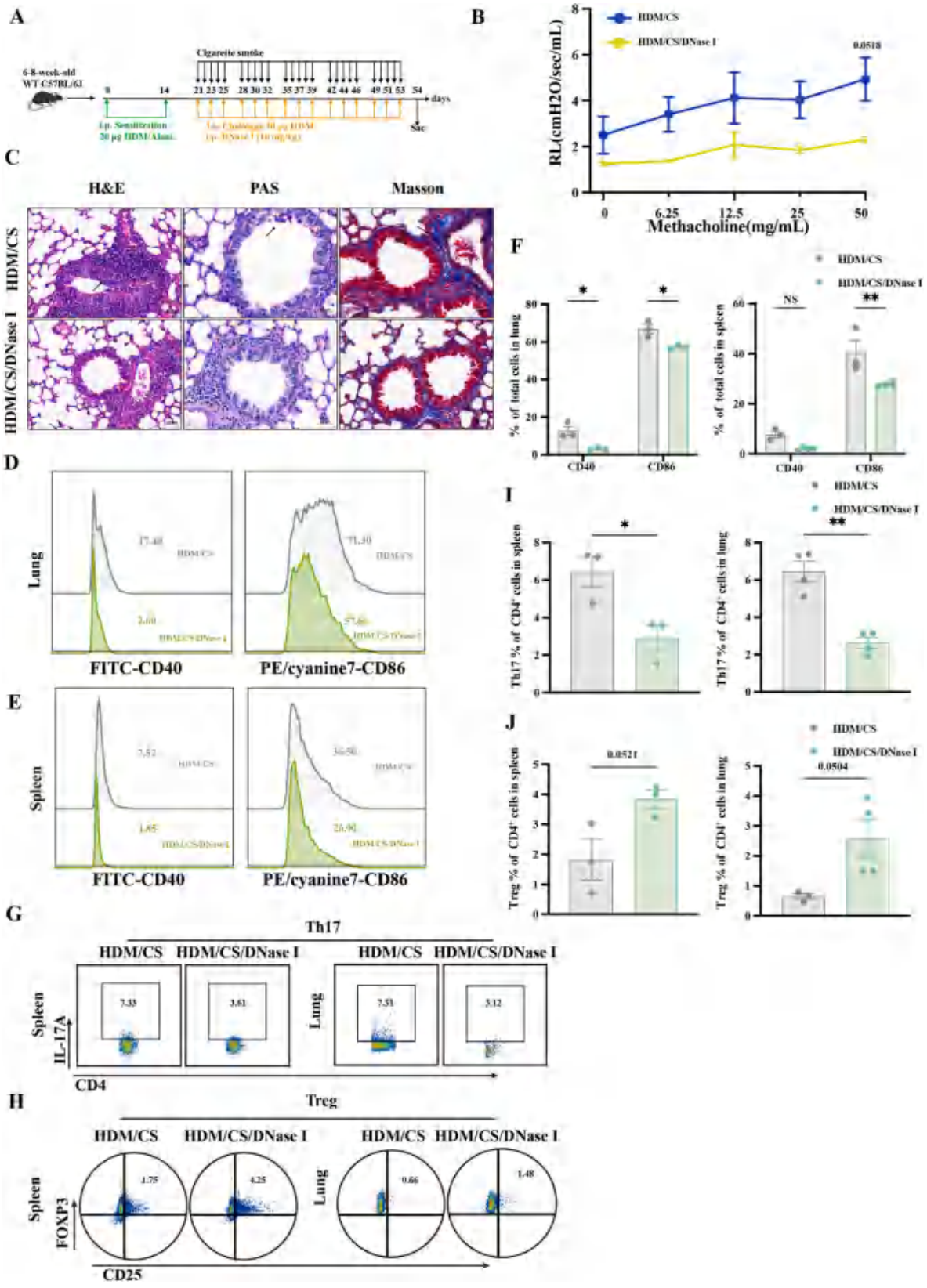

Fig. 5. NET release was related to asthma exacerbation induced by CS exposure. (A) The Strategy for DNase I treatment in the CS exposed-asthma murine model. (B) Lung resistance (R_L) was determined in response to increasing concentrations (0, 6.5, 12.5, 25, 50 mg/mL) of methacholine. (C) Representative images of histologic mice lung sections stained with H&E, PAS, and Masson (scale bars, 40 μm, arrow: typical areas). (D and E) Matured DCs ($CD45^+CD11c^+CD40^+$ and $CD45^+CD11c^+CD86^+$ cells) in the lungs and spleens of mice were analyzed by flow cytometry. (F) Quantification of CD40 and CD86 expression from panel (D) and (E). (G and H) Th17 ($CD4^+IL\text{-}17A^+$) and Treg ($CD4^+CD25^+Foxp3^+$) cells in the lungs and spleens of mice were analyzed by flow cytometry. (I and J) Quantification of Th17 cells and Treg cells from panel (G) and (H). Data represent mean with SEM. $^*P < 0.05$; $^{**}P < 0.01$.

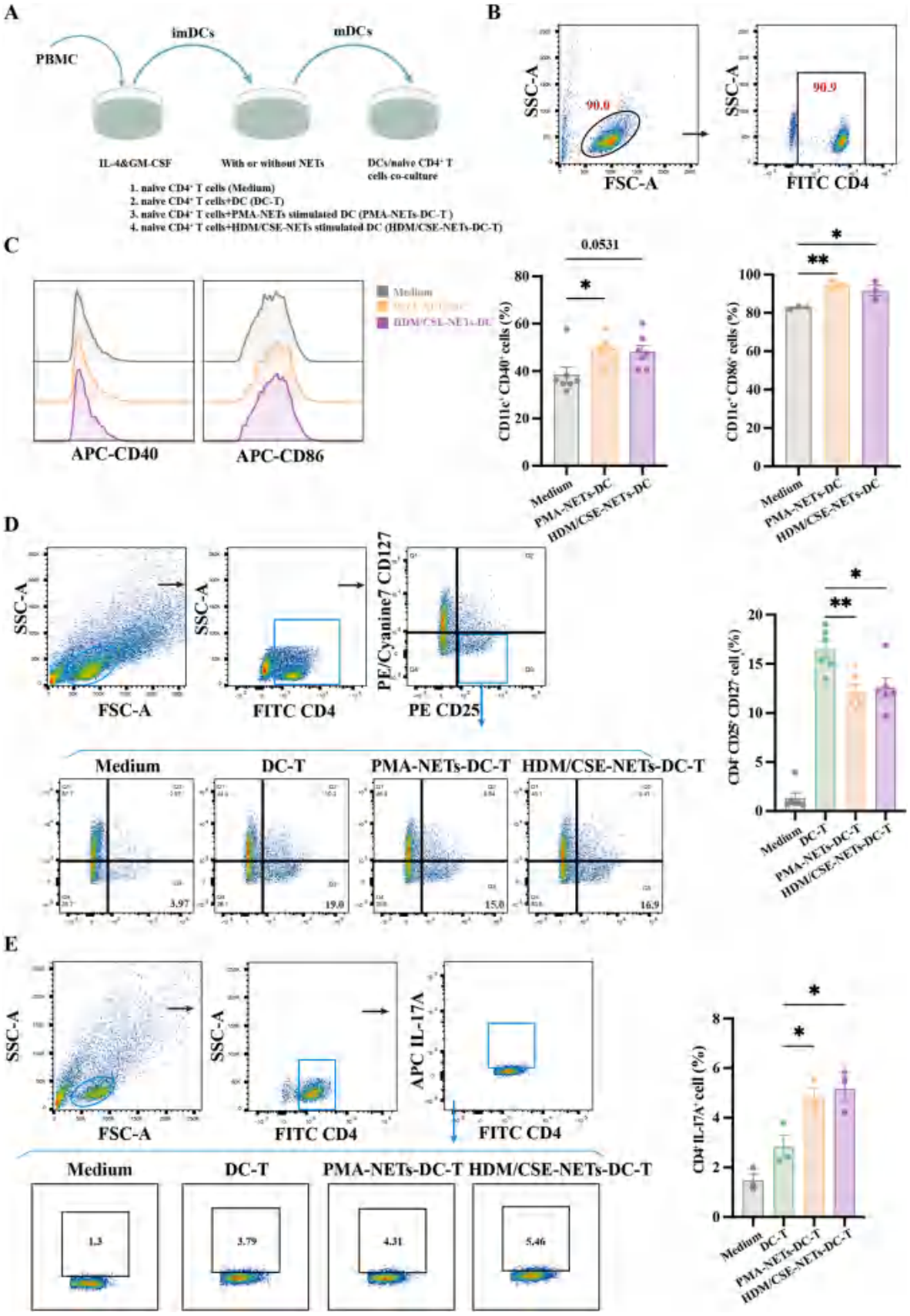

Fig. 6. HDM/CSE-induced NETs promoted the activation of DCs and influenced Th17/Treg immune imbalance *in vitro*. (A) Schematic diagram of co-culture of DCs and naïve $CD4^+$ T cells. (B) The purity of naïve $CD4^+$ T cells were detected by flow cytometry. (C) Surface expression of activation markers CD40 and CD86 on $CD11c^+$ DCs was analyzed by flow cytometry. (D and E) The proportion of Treg ($CD4^+CD25^+CD127^-$) cells and Th17 ($CD4^+IL\text{-}17A^+$) cells in the co-culture condition. Data represent mean with SEM. $^*P < 0.05$; $^{**}P < 0.01$.

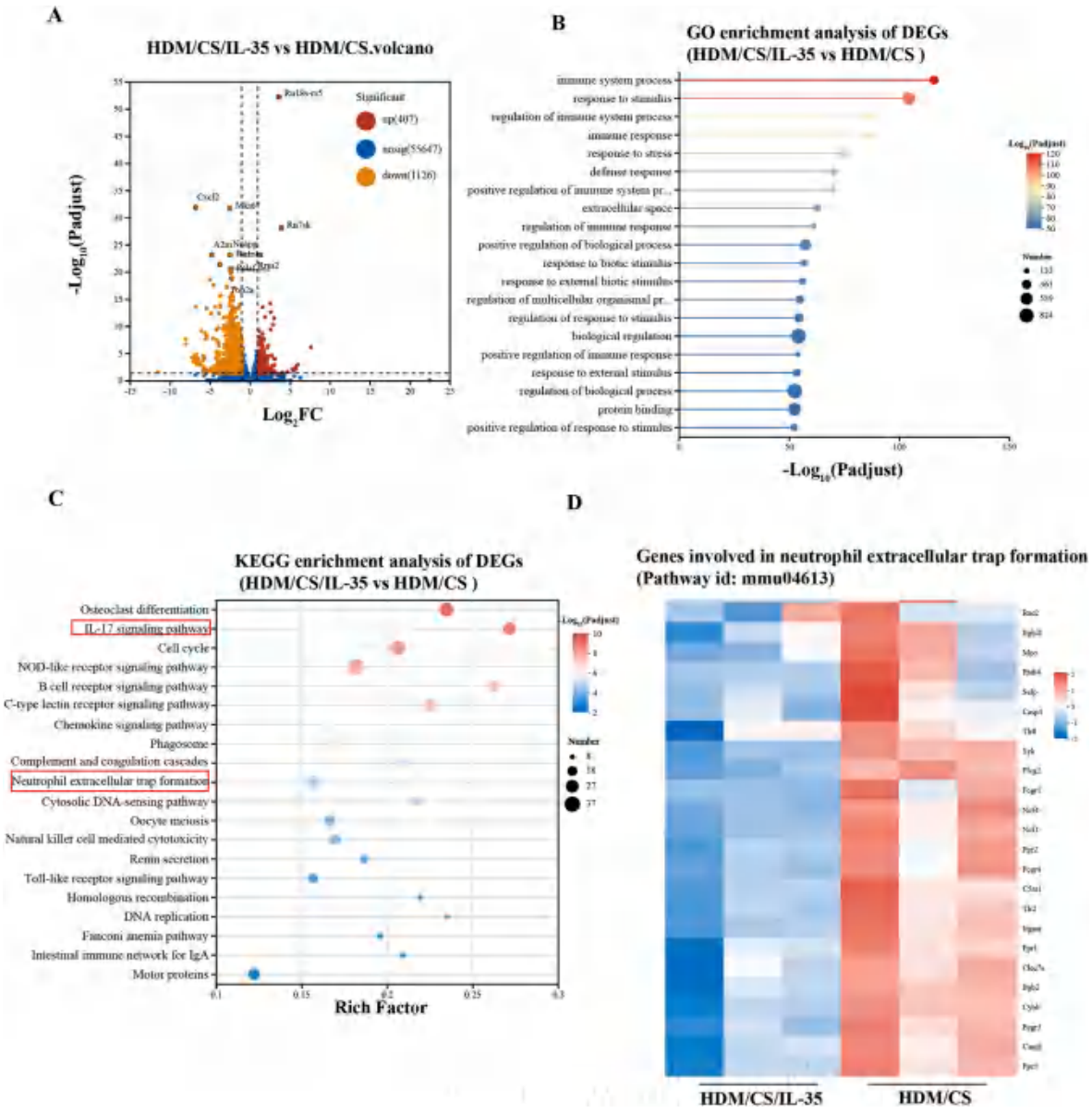

Fig. 7. RNA sequencing revealed that the mechanism of IL-35 in alleviating CS exposed-asthma exacerbation. (A) Volcano plot showing DEGs in HDM/CS/IL-35 *vs* HDM/CS mice. The up-regulated genes (red), and the down-regulated genes (yellow-brown) with a $\log_2$ (fold-change)| >1, and with $P< 0.05$. (B and C) The DEGs based on fold change were used for GO pathway and KEGG pathway analysis. (D) The genes related to the NET formation pathway, which is a defined pathway in KEGG pathways (id: mmu04613), were selected and displayed in heatmap.

activation. Notably, the ferroptosis inhibitor Fer-1 effectively suppressed HDM/CSE-induced NET formation. In contrast, Cl-amidine, a specific NET inhibitor, had no effect on ferroptosis, suggesting that ferroptosis acts upstream to regulate NET formation (Fig. 10A-I).

STAT3 overexpression has been implicated in increased NET formation in colon cancer-derived neutrophils, underscoring the critical role of the STAT3 signaling axis in regulating NET formation [39]. STAT3 is also a key regulator of ferroptosis [40,41]. In line with these findings, we observed elevated levels of p-STAT3 in the HDM/CSE group (Fig. 10J and K). To further explore the relationships among STAT3, ferroptosis, and NET formation, we transfected dHL-60 cells with a STAT3 overexpression plasmid (efficiency shown in Fig. S12). Consistent with previous reports, STAT3 overexpression enhanced both ferroptosis and NET formation (Fig. 10L-T), suggesting that increased STAT3 activation exacerbates these processes. Given the ability of IL-35 to directly inhibit NET formation, we hypothesized that IL-35 might reduce NET formation by modulating STAT3 signaling to suppress ferroptosis. Indeed, we found that STAT3 activity is crucial for the IL-35-mediated inhibition of ferroptosis-associated NET formation. As shown in Fig. 11A-L, STAT3 overexpression abolished the inhibitory effects of IL-35 on both ferroptosis and NET formation.

3.8. The gp130 receptor is a crucial subunit for the biological effects of IL-35

The IL-35 receptor consists of the gp130 and IL-12Rβ2 subunits. For IL-35 to exert its biological effects, binding to its receptor is essential, with gp130 being one of the most significant inhibitory receptors [42-44], however, the specific roles of these subunits in neutrophils remain poorly defined. Previous research has shown that the activation of gp130 can inhibit NET formation in systemic lupus erythematosus [45]. In our study, we observed greater activation of the gp130 receptor than of the IL-12Rβ2 receptor in both neutrophils and dHL-60 cells (Fig. 12A). We hypothesized that the gp130 receptor is crucial for the

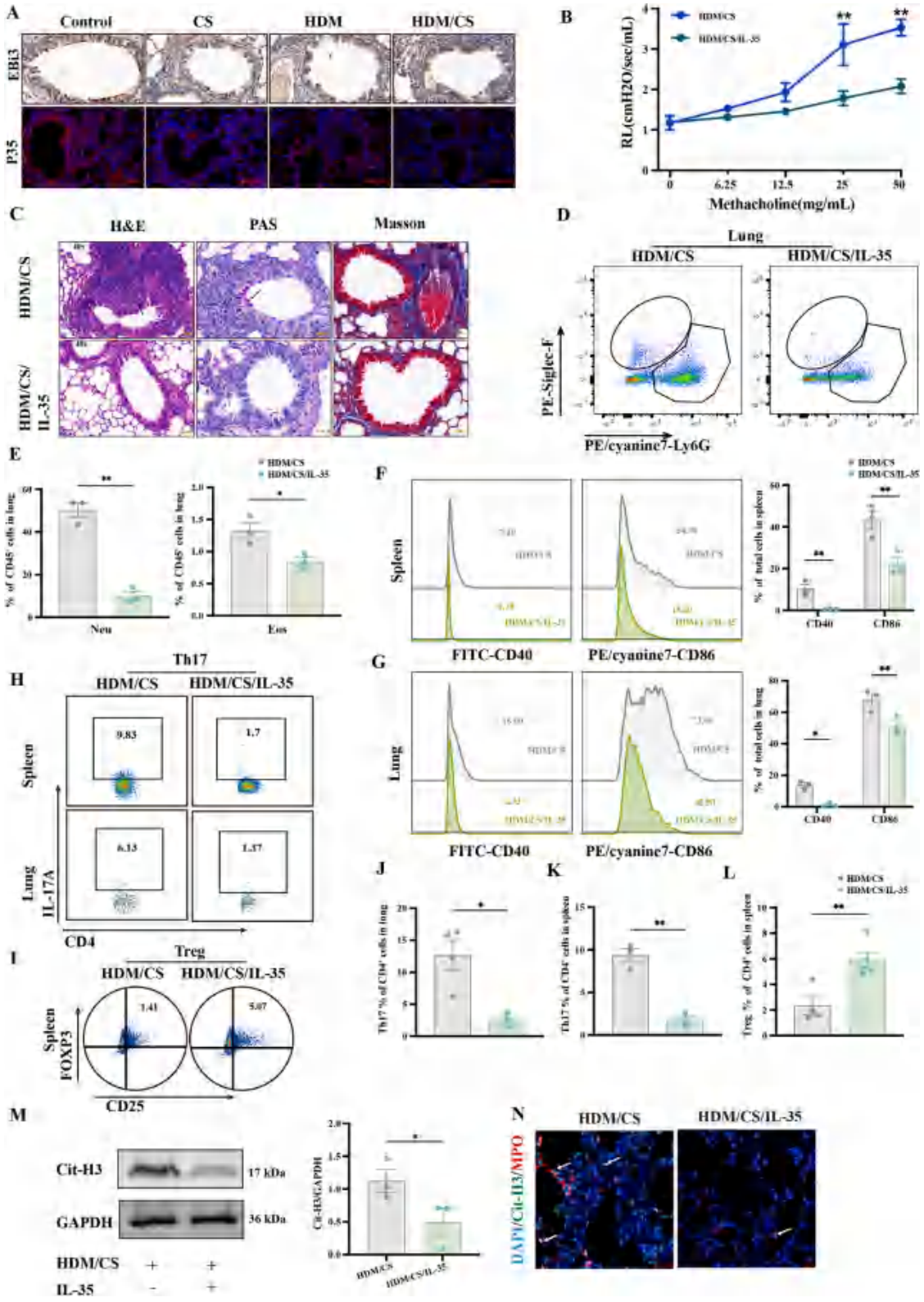

Fig. 8. IL-35 protected against CS exposed-asthma exacerbation through inhibiting NET formation. (A) Representative images of EBi3 and P35 detected by immunohistochemistry (IHC) or IF (scale bars, 50 μm). (B) Lung resistance (R_L) was determined in response to increasing concentrations (0-50 mg/mL) of methacholine. (C) Representative images of histologic mouse lung sections stained with H&E, PAS, and Masson (scale bars, 40 μm, arrow: typical areas). (D and E) Eosinophils ($CD45^+CD11^-CD11b^+SiglecF^+$) and neutrophils ($CD45^+CD11^-CD11b^+Ly6G^+$) in the lungs of mice were analyzed by flow cytometry. (F and G) Matured DCs ($CD45^+CD11c^+CD40^+$ and $CD45^+CD11c^+CD86^+$ cells) in the lungs and spleens of mice were analyzed by flow cytometry. (H-L) Th17 ($CD4^+IL\text{-}17A^+$) and Treg ($CD4^+CD25^+Foxp3^+$) cells in the lungs and spleens of mice were analyzed by flow cytometry. (M) Protein levels of Cit-H3 were measured by Western blot and analyzed by Image J. (N) Lung tissues were subjected to immunofluorescence staining with Cit-H3 (green), MPO (red), and DAPI (blue) to detect NET formation (NETs: white arrows, scale bars, 10 μm). Data represent mean with SEM. $^*P < 0.05$; $^{**}P < 0.01$.

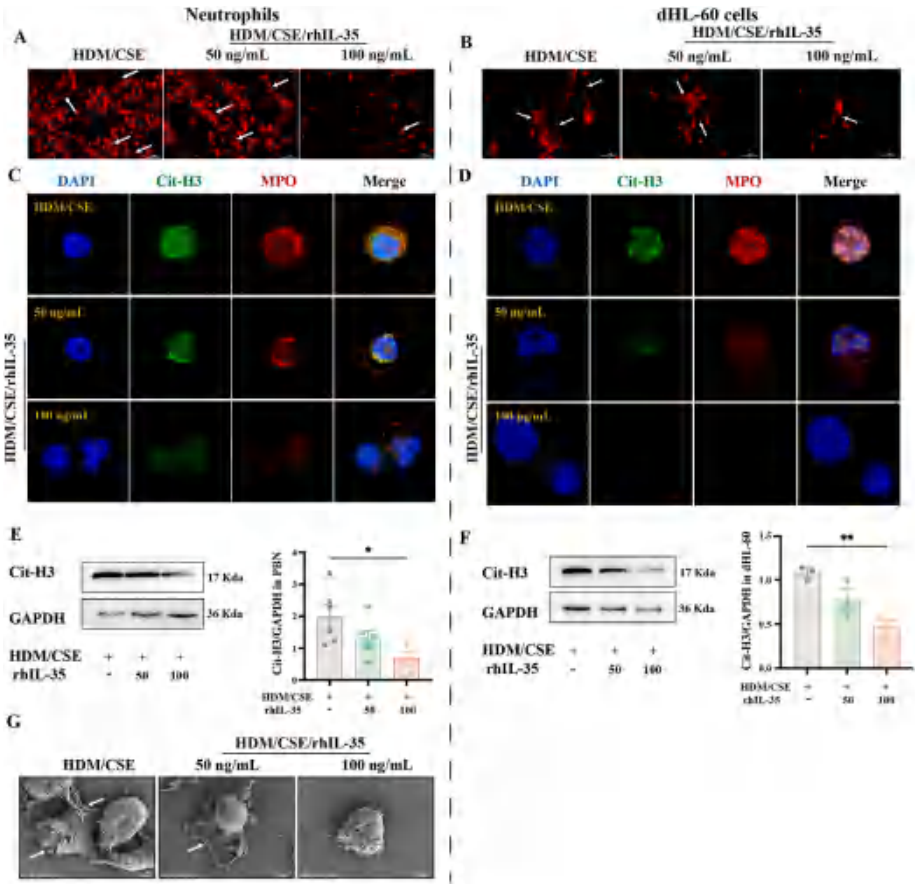

Fig. 9. IL-35 inhibited NET formation *in vitro*. (A and B) Representative immunofluorescence images of PI staining of dsDNA in neutrophils (A) and dHL-60 cells (B) (NETs: white arrows, scale bars, 50 μm). (C and D) Representative immunofluorescence staining of Cit-H3 (green), MPO (red), and DAPI (blue) to visualize NET formation in neutrophils (C) and dHL-60 cells (D) detected by confocal laser scanning microscopy (Red circle: NETs, scale bars, 50 μm). (E and F) Protein levels of Cit-H3 in neutrophils (E) and dHL-60 cells (F) were measured by Western blot and analyzed by Image J. (G) NETs were detected by scanning electron microscope in neutrophils (Scale bars, 10 μm). Data represent mean with SEM. $^{*}P < 0.05$; $^{**}P < 0.01$.

inhibitory effect of IL-35 on STAT3-mediated ferroptosis-associated NET formation. To test this hypothesis, we employed specific siRNAs to knock down gp130, and the efficiency of this knockdown was confirmed (Fig. S13). Notably, we observed that gp130 knockdown resulted in increased phosphorylation of STAT3 and a concomitant upregulation of ferroptosis and NETs (Fig. 12B-N). These findings imply that activation of the gp130 receptor is essential for IL-35 to exert its biological effect.

3.9. The gp130/STAT3 axis governs the IL-35-mediated control of inflammation and NET formation

To dissect the mechanistic role of the gp130/STAT3 axis in IL-35-mediated effects, we administered SC144, a selective gp130 inhibitor, or Colivelin TFA, a STAT3 activator, alongside IL-35 to mice with CS exposed-asthma (Fig. 13A). We observed that SC144 led to a significant worsening of AHR, whereas Colivelin TFA had no effect (Fig. 13B). Histological analysis revealed that disruption of the gp130/STAT3 pathway partially reversed the pathological improvements mediated by IL-35 (Fig. 13C). We next assessed how modulation of the gp130/STAT3 axis influences immune responses, particularly DC maturation and T-cell differentiation, during IL-35 treatment. SC144 led to an increase in CD40 expression and CD86, while Colivelin TFA resulted in increased CD86 levels (Fig. 13D). Both interventions shifted T-cell differentiation toward Th17 cells and concurrently suppressed the expansion of Treg cells (Fig. 13E-I). This shift in immune balance was coupled with increased ferroptosis and NET formation (Fig. 13J-L). These data further indicate that IL-35 inhibits ferroptosis-associated NETs and promotes disease remission in response to CS exposure, which is at least partly dependent on the gp130/STAT3 axis.

3.10. Serum NET expression is increased in smokers with asthma and is positively correlated with pulmonary function severity

The serum NET levels in asthmatic patients (see Table S1 for details on general characteristics) were assessed and we observed significantly higher MPO-DNA levels in smokers with asthma than in nonsmokers with asthma and healthy controls, and the serum HMGB-1 and NE levels were elevated in the smokers with asthma (Fig. 14A). Moreover, the serum levels of IL-17A and IL-35 were measured (Fig. 14B), revealing elevated IL-17A expression in smokers with asthma, whereas IL-35 levels were reduced. MPO-DNA, HMGB-1, and NE levels were negatively correlated both with FEV_1/pred and FEV_1/FVC (Fig. 14C-H). IL-17A levels were positively correlated with MPO-DNA and HMGB-1 levels (Fig. 14I-K), and IL-35 levels showed a negative correlation trend with NET markers (Fig. 14L-N). Importantly, serum IL-35 levels showed a significant positive correlation with FEV_1/FVC. (Fig. 14O and P). In summary, our analysis of clinical serum samples indicated that elevated NET levels may be associated with T-lymphocyte polarization and worsening lung function.

4. Discussion

In this study, we demonstrated that during the CS exposed-asthma exacerbation, airway neutrophils primarily exert their biological

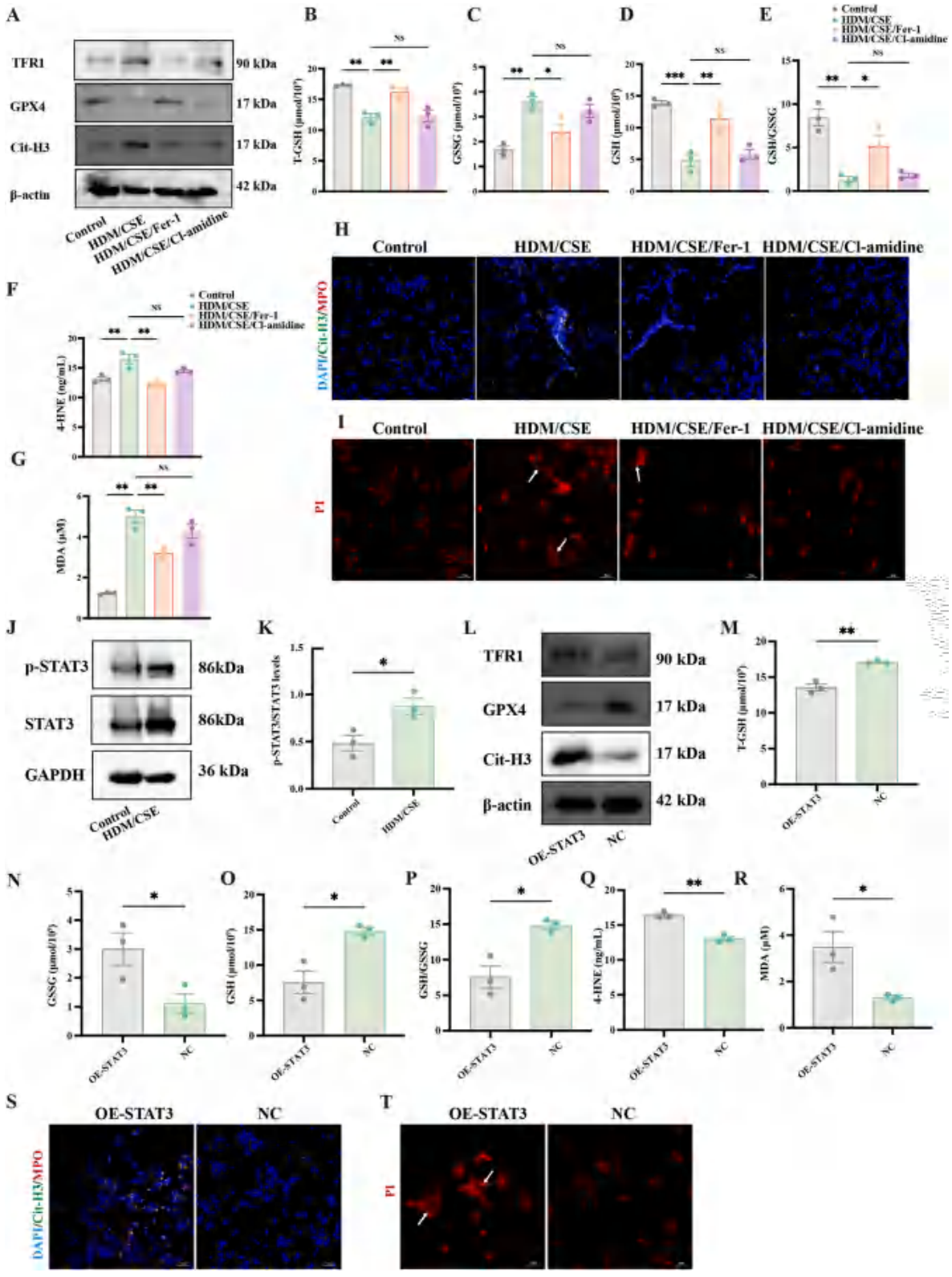

Fig. 10. The STAT3/ferroptosis axis promoted NET formation. (A) Protein levels of TFR1, GPX4, and Cit-H3 were measured by Western blot. (B-E) Levels of T-GSH, GSSG, GSH, and GSH/GSSG were measured by T-GSH/GSSG colorimetric assay kit. (F) Levels of 4-HNE were measured by 4-HNE ELISA kit. (G) Levels of lipid peroxidation was measured by MDA assay. (H) Representative immunofluorescence staining of Cit-H3 (green), MPO (red), and DAPI (blue) to visualize NET formation in neutrophils (scale bars, 50 μm). (I) Representative immunofluorescence images of PI staining of dsDNA (NETs: white arrows, scale bars, 50 μm). (J and K) Protein levels of p-STAT3/STAT3 were measured by Western blot and analyzed by Image J. (L) Protein levels of TFR1, GPX4, and Cit-H3 were measured by Western blot. (M-P) Levels of T-GSH, GSSG, GSH, and GSH/GSSG were measured by T-GSH/GSSG colorimetric assay kit. (Q) Levels of 4-HNE were measured by 4-HNE ELISA kit. (R) Levels of lipid peroxidation was measured by MDA assay. (S) Representative immunofluorescence staining of Cit-H3 (green), MPO (red), and DAPI (blue) to visualize NET formation (scale bars, 50 μm). (T) Representative immunofluorescence images of PI staining of dsDNA (NETs: white arrows, scale bars, 50 μm). Data represent mean with SEM. $^{*}P < 0.05$; $^{**}P < 0.01$.

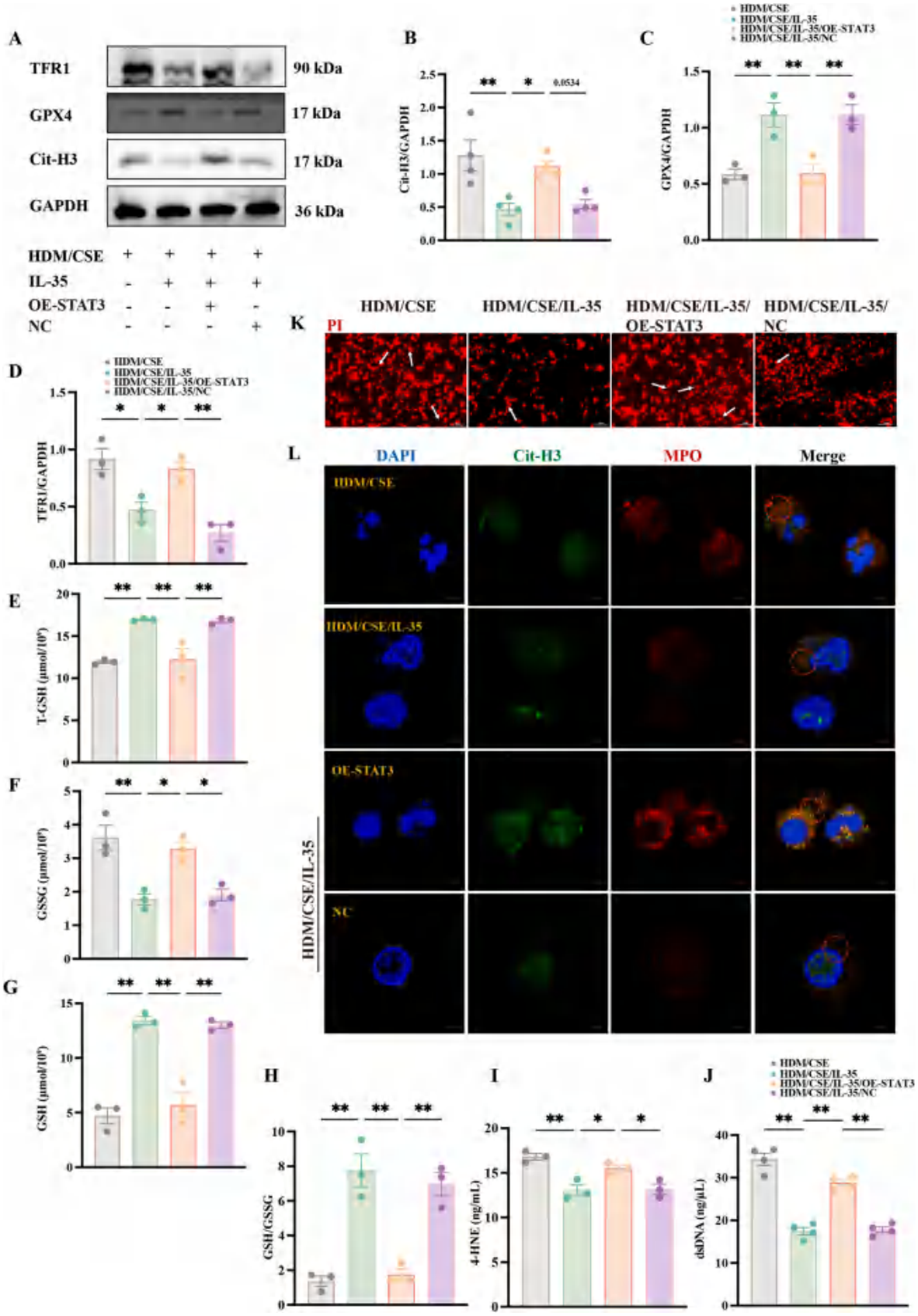

Fig. 11. IL-35 modulated STAT3 to inhibit ferroptosis-associated NET formation. (A-D) Protein levels of TFR1, GPX4, and Cit-H3 were measured by Western blot and analyzed by Image J. (E-H) Levels of T-GSH, GSSG, GSH, and GSH/GSSG were measured by T-GSH/GSSG colorimetric assay kit. (I) Levels of 4-HNE were measured by 4-HNE ELISA kit. (J) The concentration of dsDNA was quantified using a NanoDrop one. (K) Representative immunofluorescence images of PI staining of dsDNA (NETs: white arrows, scale bars, 50 μm). (L) Representative immunofluorescence staining of Cit-H3 (green), MPO (red), and DAPI (blue) to visualize NET formation in neutrophils (Red circle: NETs, scale bars, 50 μm). Data represent mean with SEM. $^{*}P < 0.05$; $^{**}P < 0.01$.

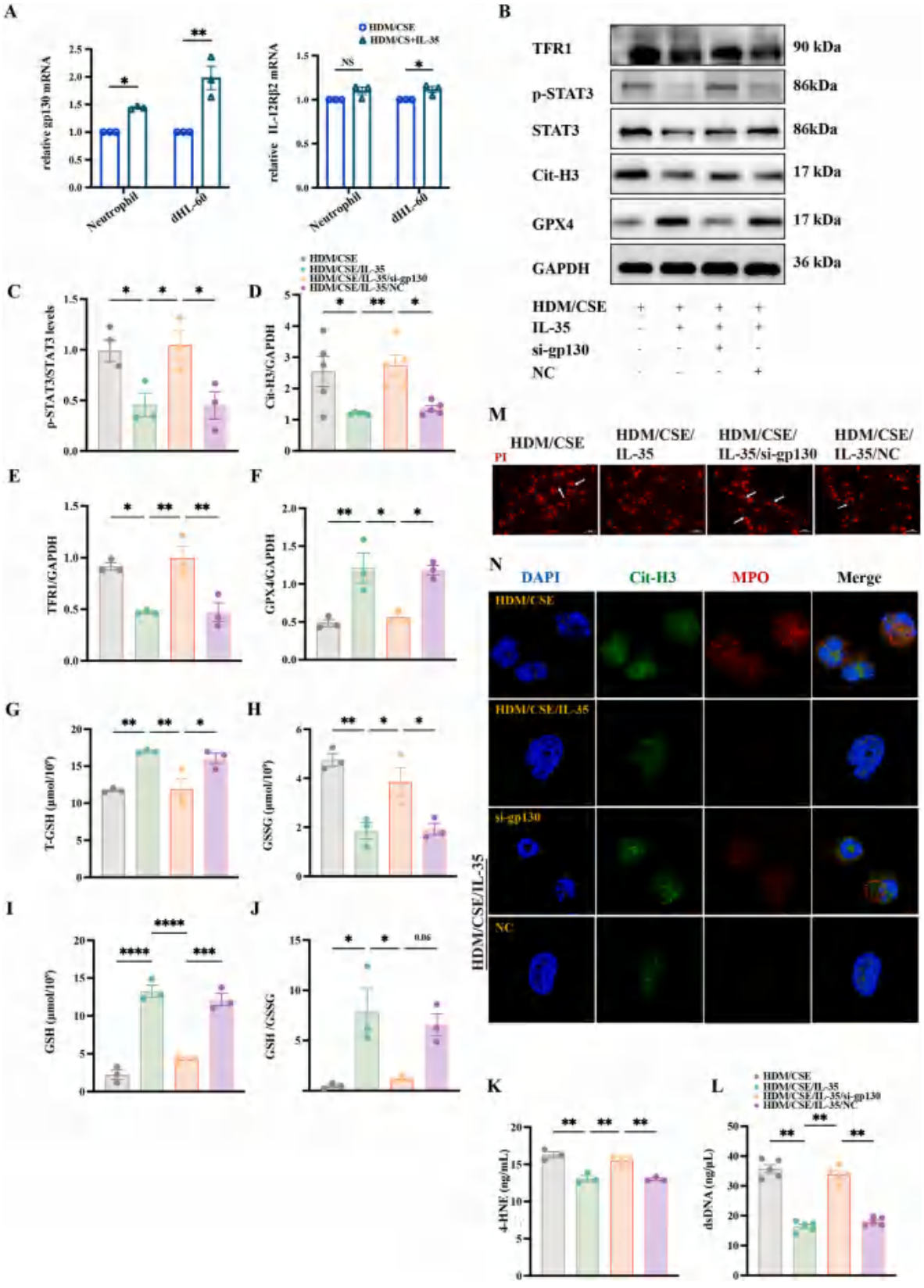

Fig. 12. The gp130 receptor was a key component required for IL-35 to exert its biological effects. (A) Expression levels of gp130 and IL-12Rβ2 receptors on the surface of neutrophils and dHL-60 cells following IL-35 stimulation. (B-F) Representative Western blot and quantification analysis of protein expression of STAT3, p-STAT3, GPX4, TFR1, and Cit-H3. (G-J) Levels of T-GSH, GSSG, GSH, and GSH/GSSG were measured by T-GSH/GSSG colorimetric assay kit. (K) Levels of 4-HNE were measured by 4-HNE ELISA kit. (L) The concentration of dsDNA was quantified using a NanoDrop one. (M) Immunofluorescence images of PI staining of dsDNA were shown (NETs: white arrows; scale bars, 50 μm). (N) Representative immunofluorescence staining of Cit-H3 (green), MPO (red), and DAPI (blue) to visualize NET formation detected by confocal laser scanning microscopy (Red circle: NETs, scale bars, 50 μm). Data represent mean with SEM. $^{*}P < 0.05$; $^{**}P < 0.01$.

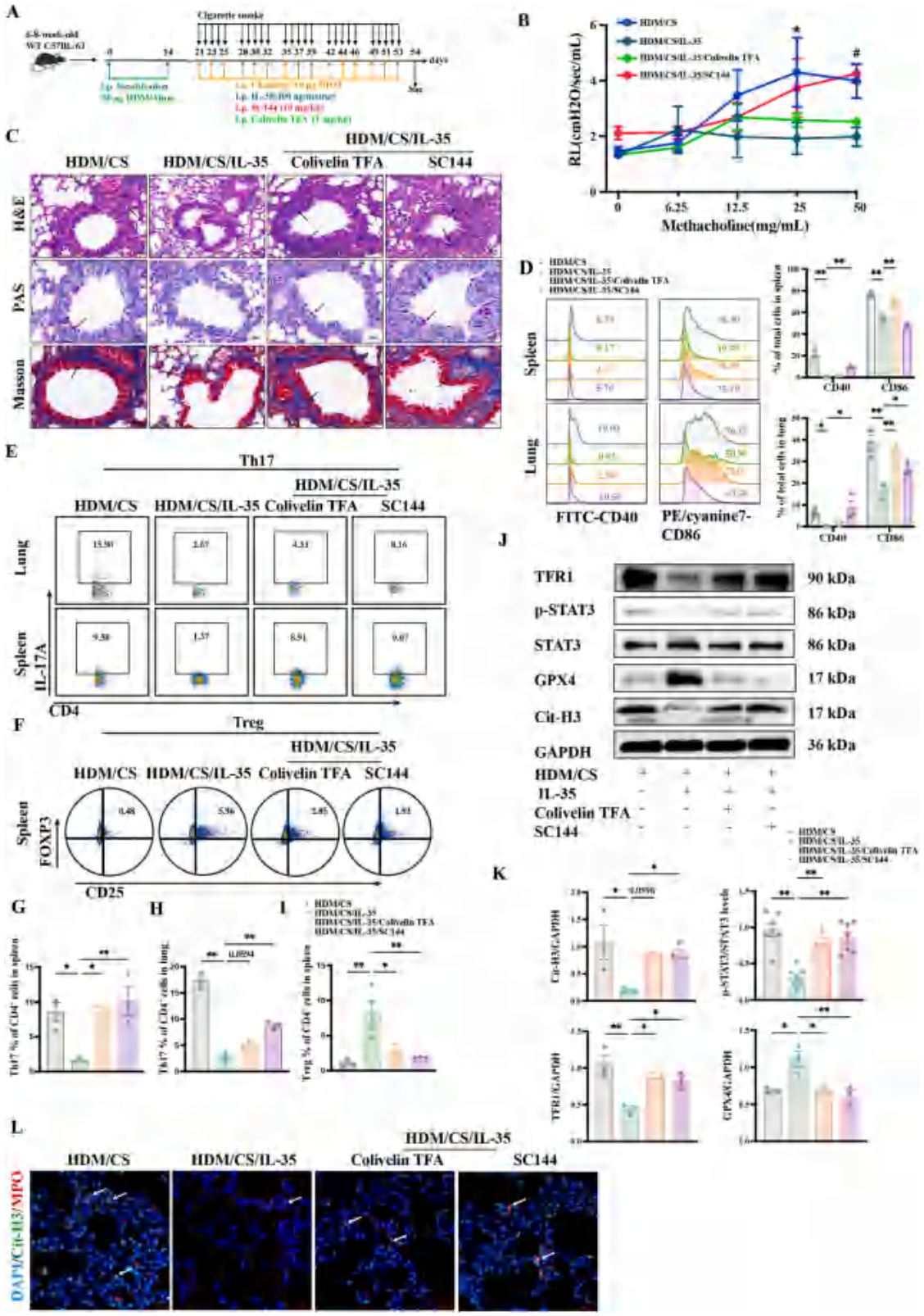

Fig. 13. Blockade of the gp130/STAT3 axis counteracts the beneficial effects of IL-35 *in vivo*. (A) The Strategy for targeting gp130/STAT3 axis in the HDM/CS/IL-35 group mice. (B) Lung resistance (R_L) was determined in response to increasing concentrations (0-50 mg/mL) of methacholine. (C). Representative images of histologic mice lung sections stained with H&E, PAS, and Masson (scale bars, 40 μm, arrow: typical areas). (D) Matured DCs ($CD45^+CD11c^+CD40^+$ and $CD45^+CD11c^+CD86^+$ cells) in the lungs and spleens of mice were analyzed by flow cytometry. (E-I) Th17 ($CD4^+IL\text{-}17A^+$) and Treg ($CD4^+CD25^+Foxp3^+$) cells in the lungs and spleens of mice were analyzed by flow cytometry. (J and K) Protein levels of Cit-H3, GPX4, TFR1, STAT3, and p-STAT3 were measured by Western blot and analyzed by Image J. (L) Lung tissues were subjected to immunofluorescence staining with Cit-H3 (green), MPO (red), and DAPI (blue) to detect NET formation (NETs: white arrows, scale bars, 10 μm). Data represent mean with SEM. $^*P < 0.05$; $^{**}P < 0.01$.

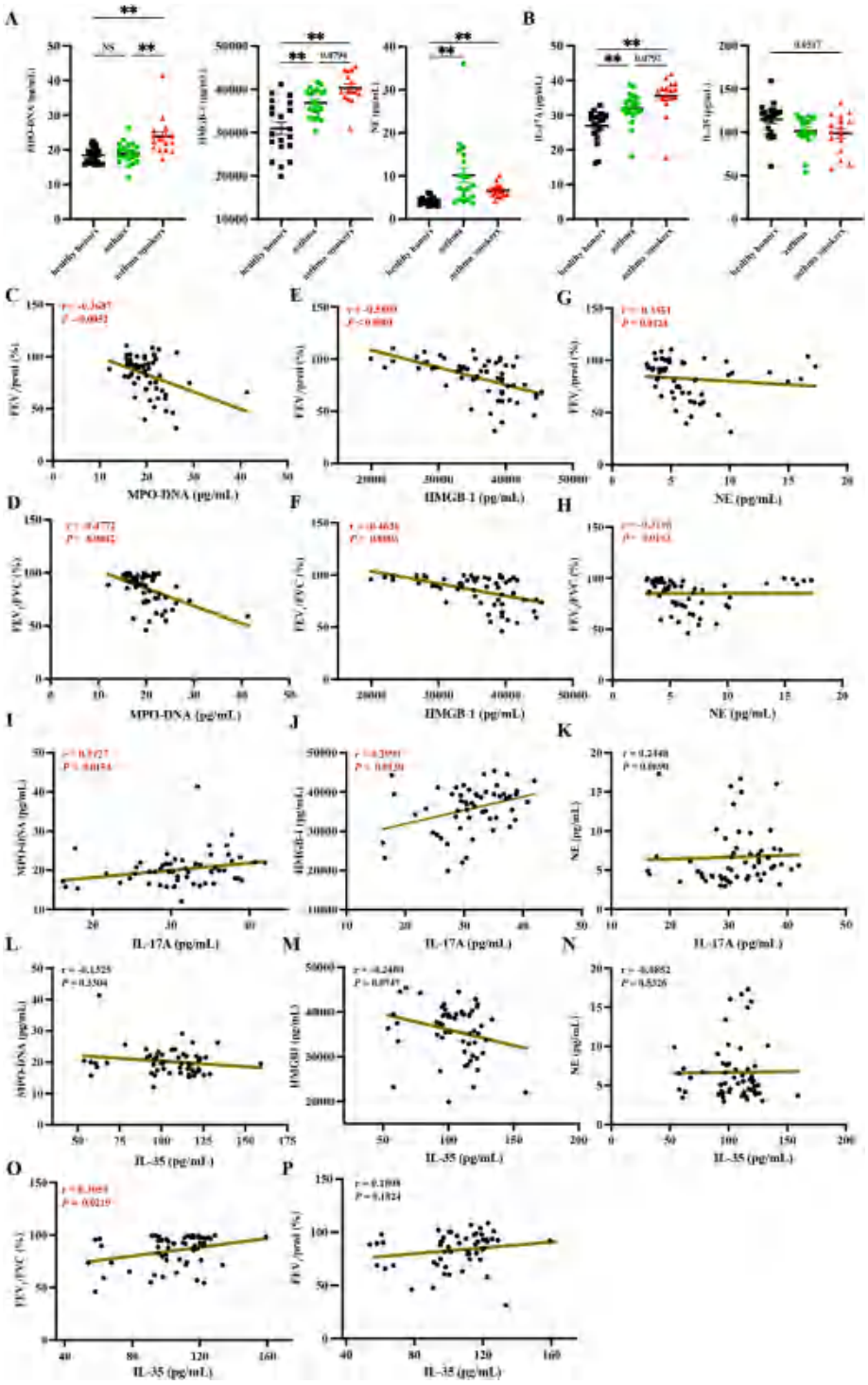

Fig. 14. Positive correlation between NETs and pulmonary function severity. (A and B) The concentrations of MPO-DNA, NE, HMGB-1, IL-17A and IL-35 in human serum were detected by ELISA. (C-H) The correlation between MPO-DNA, HMGB-1, NE and FEV_1/pred or FEV_1/FVC. (I-N) The correlations of IL-17A and IL-35 with MPO-DNA, HMGB-1, and NE, respectively. (O-P) The correlations of IL-35 with FEV_1/FVC and FEV_1/pred.

effects through NET formation. Specifically, NETs exacerbate the inflammatory response by influencing the DC-Th17/Treg immune imbalance, highlighting NETs as "linchpin" linking innate and adaptive immunity. In addition, our findings reveal a novel function of IL-35 in protecting against neutrophilic inflammation via inhibition of NETs via the gp130/STAT3/ferroptosis axis.

Research has indicated that 44 % of patients with severe asthma on biologics are former smokers and 1 % are current smokers [46]. Despite a gradual decline in smoking rates over time, exposure to secondhand smoke continues to cause harm to nonsmokers [47]. CS exacerbates asthma severity and confers multifaceted adverse clinical outcomes [48]. Multiple publications have reported that heavy smokers exhibit more severe obstructive impairments, demonstrating steroid insensitivity, thus representing a distinct non-T2 phenotype [49]. In addition, glucocorticoid steroid treatment failed to reduce neutrophilic inflammation in sensitized mice exposed to CS [50]. An observation in our experimental framework was the absence of significant pathological differences between the CS and control group, suggesting that CS

exposure alone may not suffice to initiate full asthma-like pathogenesis under the current exposure regimen. Importantly, when compared with CS exposure alone, the combined HDM/CS challenge exhibited markedly elevated AHR, airway and peripheral vascular inflammatory cell infiltration, mucus secretion, and collagen fiber deposition, with increased antigen presentation by DCs, increased Th17 cells, and decreased Treg cells, which indicated that a disrupted immune balance contributed to the exacerbation of asthma. Furthermore, neutrophils, key players in innate immunity and type 17 responses, were markedly elevated in the HDM/CS group, contributing significantly to the poor prognosis of individuals with CS exposed-asthma exacerbation.

An exaggerated or persistent neutrophilic response is implicated in the pathology of severe asthma, and neutrophils are therefore attractive therapeutic targets. Research has reported that neutrophil depletion alleviates PM2.5-induced mucus hypersecretion in individuals with asthma [51]. However, therapeutic strategies aimed at reducing neutrophilic inflammation may not fully account for the regulatory roles that neutrophils play. In our study, neutrophil depletion with anti-Ly6G antibodies had no effect on the key pathological features of asthma. In addition, anti-Ly6G treatment did not result in significant changes in DC maturation or the differentiation of Th17 and Treg cells compared with IgG2a isotype controls. Interestingly, we observed a notable increase in eosinophil numbers in the anti-Ly6G group, which is consistent with findings from Patel et al. [51] and Whitehead GS et al. [52], who both reported that neutrophil depletion exacerbates allergic inflammation in asthma models. The inability of neutrophil depletion to mitigate inflammation may stem from a compensatory remodeling of the pulmonary inflammatory network under cigarette exposure. Neutrophils may play dual roles in CS exposed-asthma: on one hand, they drive tissue damage by releasing MPO and NETs [53]; on the other hand, they secrete lipoxin A4 (LXA4), which inhibits the production of eosinophil chemoattractant eotaxin [54]. This paradoxical function suggests that indiscriminate depletion of neutrophils may disrupt the innate immune balance. Indeed, our experiments observed a rebound increase in eosinophils, possibly due to the loss of neutrophil-derived inhibitory factors such as LXA4, leading to excessive activation of the IL-5/IL-13 pathway [55]. Notably, recent studies have identified unique neutrophil subpopulations, some of which highly express PD-L1 and suppress $CD4^+$ T cell activation [56]. The traditional anti-Ly6G antibody may selectively deplete pro-inflammatory subsets while sparing regulatory populations, limiting its overall depletion efficiency. These mechanisms collectively suggest that under cigarette exposure, neutrophils are not merely effector cells but key nodes in a complex immune regulatory network. Future therapeutic strategies may need to target specific neutrophil subpopulations while concurrently intervening in compensatory pathways, rather than broadly depleting all neutrophils.

The ineffectiveness of neutrophil depletion therapy led us to further explore the role of neutrophils. In our study, RNA sequencing revealed significant enrichment of the NET pathway and marked upregulation of NET-related genes in the HDM/CS group. The increase in NETs then was confirmed both *in vivo* and *in vitro*. These results indicate that neutrophils primarily exert their effects through the release of NETs. We further demonstrated that NET-related biomarkers (MPO-DNA, HMGB1, and NE) in the serum were increased in smokers with asthma compared with healthy control subjects, related to deteriorated lung function. In fact, the presence of uncontrolled NETs has a detrimental effect on neutrophilic asthma [20]. NETs and their histones promote Th17 cell differentiation directly via TLR2/MyD88 [57], or by activating DCs to indirectly influence the differentiation of naïve $CD4^+$ T cells into Th17 cells [58]. However, due to their considerable destructive capacity and potential to cause damage to healthy tissue, it is critical that NETs homeostasis be tightly regulated. In our study, CS exposed-asthma was alleviated after NETs were disrupted by DNase I treatment. In this context, the targeted degradation of NETs, rather than neutrophil depletion, might be a potential therapeutic strategy that blocks the negative effects of neutrophils without altering their beneficial functions. However, the clinical translation of NET-targeted therapies remains limited by significant challenges, particularly with respect to safety and efficacy, underscoring the need for safer and more precise biomolecular interventions.

IL-35 is produced mainly by Treg cells [59] and reversibly suppresses allergic inflammation and IL-17-dependent AHR [23]. Transfected MSCs overexpressing IL-35 significantly improved the control of symptoms in an allergic asthma model [60]. We also showed that Ad-IL-35 attenuated Th17-associated inflammation by downregulating the TSLP-DC axis in mice with CS exposed-asthma [11]. However, whether IL-35 regulates NET formation has not been reported. In this study, through transcriptomic sequencing as well as comprehensive *in vivo* and *in vitro* experiments, we provide robust evidence that IL-35 inhibits NET formation and thereby alleviates DC-Th17/Treg immune imbalance as well as neutrophilic inflammation, which not only increases our understanding of the immunomodulatory role of IL-35 but also highlights the significant potential of IL-35 as a therapeutic target for the clinical management of CS exposed-asthma. In future research, it is required to systematically evaluate the biosafety and pharmacokinetic properties of recombinant IL-35 protein. To enhance therapeutic precision, using biodegradable nanocarriers for pulmonary-targeted has the potential to optimize drug stability, bioavailability, while simultaneously minimizing systemic off-target effects. Furthermore, combining IL-35 with existing targeted therapies (e.g., anti-IL-5, anti-IL-5R or anti-IL-4R) may synergistically attenuate inflammation and restore Th17/Treg homeostasis, offering a multi-target therapeutic strategy for CS exposed-asthma.

In some diseases, the processes of NET formation and ferroptosis are activated through common mechanisms and shared signaling pathways, such as oxidative stress and activation of the STAT family of transcription factors [34,38]. Investigating the interaction between ferroptosis and NETs is crucial for understanding immune responses, inflammatory processes, and the underlying mechanisms of related diseases. Previous studies have focused predominantly on the impact of NET release on ferroptosis in target cells or tissues [38,61,62]. In contrast, our study provides an expanded perspective by revealing the interconnected relationship between ferroptosis and NET formation within the neutrophils in a murine of CS exposed-asthma.

The STAT family mediates IL-35 signaling, and IL-35 utilizes the STAT network to transduce signals to the nucleus, thereby enhancing the plasticity of cellular and tissue responses [44]. Recent research has shown that IL-35 enhances the phosphorylation of STAT1 and STAT4, which competitively bind to the recognition region of STAT3, thereby inhibiting STAT3-mediated fibrosis [63]. STAT3 exhibits a dual role in ferroptosis regulation. On one hand, it promotes lipid peroxidation and induces ferroptosis [64]; on the other hand, it inhibits ferroptosis by stabilizing GPX4 [65,66]. This dual role of STAT3 in ferroptosis regulation highlights its context-dependent functionality across different diseases and cell subtypes. However, it remains unclear whether p-STAT3 mediates ferroptosis in neutrophils from CS exposed-asthma and if IL-35 plays a role in modulating the STAT3-ferroptosis axis. In this study, we observed that in mice with CS exposed-asthma, increased STAT3 phosphorylation was associated with elevated levels of ferroptosis and NETs and that IL-35 restricted ferroptosis. More importantly, IL-35-mediated protection from ferroptosis and NETs was abolished by a STAT3 activator and by OE-STAT3. This finding is consistent with the report by Li Yuanyuan et al., which demonstrated that inhibiting STAT3 phosphorylation in neutrophils alleviates NET formation and mitigates lung inflammation in a mouse model of acute lung injury [67]. Together, our results suggest that STAT3 is a key transcription factor mediating the beneficial effects of IL-35.

Thus, it is essential to identify the receptors that inhibit STAT3 phosphorylation in neutrophils in response to IL-35. IL-35 consists of two subunits, p35 and EBI3, which interact with the receptor subunits IL-12Rβ2 and gp130 to form various receptor complexes. Diverse receptor combinations (e.g., IL-12Rβ2/IL-12Rβ2, IL-12Rβ2/gp130, and

gp130/gp130) may exist in different diseases, providing a structural basis for the functional diversity of IL-35 and making the receptor subunit preference of IL-35 a highly valuable research direction [42]. In cardiac transplantation, research indicates that IL-35 activation of the gp130 receptor stabilizes the Treg phenotype, thereby improving $CD8^+$ T cell infiltration in allografts [43]. However, in experimental autoimmune uveitis, IL-35 activates the IL-12Rβ2 receptor, promotes B cell proliferation and enhances the regulation of the immune response [68]. In our study, the mRNA expression of the gp130 receptor is significantly higher than that of IL-12Rβ2 after IL-35 treatment, suggesting that gp130 play a dominant role in IL-35 signal transduction. Blockade of gp130 signaling with SC144 or si-gp130 prevented the IL-35-mediated reduction in p-STAT3 levels and ferroptosis-associated NET formation. Thus, it is reasonable to speculate that it is through the gp130/STAT3/ferroptosis/NET axis that IL-35 confers its protective effects. In fact, IL-35 also exhibits diverse regulatory roles across multiple diseases. In rheumatoid arthritis, exogenous IL-35 alleviates inflammation by suppressing IFN-γ and IL-17 while boosting IL-10 secretion from Treg cells [69]. In Con A-induced hepatitis, IL-35-modified mesenchymal stem cells enhance therapeutic outcomes via the JAK1-STAT1/STAT4 pathway [70]. Similarly, IL-35 maintains Th17/Treg balance and dampens pathogen-driven immune responses in multiple sclerosis, systemic lupus erythematosus, and inflammatory bowel disease [71], consistent with its T-cell modulatory effects observed in our study. However, none of these studies implicated STAT3/ferroptosis as a mediator, underscoring the novelty of our work. Additionally, IL-35 mitigates neuropathic pain by modulating microglial phenotypes, increasing IL-10, and suppressing IL-9 and MCP-1 [72]. These findings complement our results, emphasizing IL-35's functional versatility across cell types. In addition, the mechanism identified in our study differs significantly from those in other diseases due to the distinct phenotype of this disease. This highlights the urgent need to tailor therapeutic strategies based on disease-specific pathological landscapes and signaling pathways.

Naturally, certain limitations must be acknowledged. To minimize heterogeneity, we exclusively used female mice, which may limit the generalizability of our findings to males. Future studies incorporating both sexes would be valuable to confirm the universality of the observed mechanisms. In addition, this study has several other limitations. One major limitation is that, although we have extensively validated the key role of the gp130/STAT3 axis in the IL-35-mediated regulation of ferroptosis-related NETs through pharmacological interventions *in vitro*, which strongly supports the reliability of our findings, future validation using neutrophil-specific knockin or knockout mouse models would further strengthen our conclusions. Another limitation is the small sample size of clinical samples, which prevented us from establishing a statistically significant correlation between serum IL-35 levels and lung function deterioration, although a negative correlation trend was observed.

5. Conclusion

In conclusion, we propose a novel mechanism whereby IL-35, through its dependence on neutrophil gp130 receptors, interacts with STAT3 to regulate ferroptosis-associated NETs. This interaction plays a key role in alleviating the DC-Th17/Treg imbalance and neutrophilic inflammation. These findings establish a biological basis for the potential application of IL-35 in the treatment of exacerbated of CS exposed-asthma and open new avenues for exploring its potential targets in clinical applications.

CRediT authorship contribution statement

Peizhi Tao: Writing – original draft, Methodology, Investigation, Formal analysis, Conceptualization. **Beiting Su:** Writing – original draft, Methodology, Formal analysis, Conceptualization. **Xueyan Mao:** Writing – original draft, Methodology, Formal analysis, Conceptualization. **Yusen Lin:** Formal analysis. **Li Zheng:** Investigation. **Xiaoling Zou:** Data curation. **Hailing Yang:** Data curation. **Jing Liu:** Writing – review & editing, Supervision. **Hongtao Li:** Writing – review & editing, Supervision.

Data and materials availability

The raw RNA-Seq data have been deposited in the NCBI SRA database under accession number PRJNA1199157.

Funding

This study was funded by grants from National Natural Science Foundation of China (No. 82370034) and Science and Technology Program of Guangzhou, China (No. 2024A03J0173).

Declaration of competing interest

The authors declare that they have no known competing financial interests or personal relationships that could have appeared to influence the work reported in this paper.

Acknowledgments

The authors thank Prof. Kefang Lai and Dr. Chuqin Huang for their technical support in assessing lung function in mice.

Appendix A. Supplementary data

Supplementary data to this article can be found online at https://doi.org/10.1016/j.redox.2025.103594.

Abbreviations

CS, cigarette smoke; CSE, cigarette smoke extract; HDM, house dust mite; BALF, bronchoalveolar lavage fluid; AHR, airway hyperreactivity; STAT3, Signal transducer and activator of transcription 3; HRP, horseradish peroxidase; ROS, reactive oxygen species; PBMCs, peripheral blood mononuclear cells; DCs, dendritic cells; DNase I, Deoxyribonuclease I; PMA, phorbol 12-myristate 13-acetate; GM-CSF, granulocyte-macrophage colony stimulating factor; NETs, neutrophil extracellular traps; PBNs, Peripheral blood neutrophils; DEGs, differentially expressed genes; 4-HNE, 4-Hydroxynonenal; T-GSH, Total Glutathione; GSSG, Oxidized Glutathione.

Data availability

Data will be made available on request.

References

[1] F. Schleich, N. Bougard, C. Moermans, M. Sabbe, R. Louis, Cytokine-targeted therapies for asthma and copd, Eur. Respir. Rev. 32 (2023) 220193, https://doi.org/10.1183/16000617.0193-2022.
[2] G.B.D.C.R.D. Collaborators, Global, regional, and national deaths, prevalence, disability-adjusted life years, and years lived with disability for chronic obstructive pulmonary disease and asthma, 1990-2015: a systematic analysis for the global burden of disease study 2015, Lancet Respir. Med. 5 (2017) 691–706, https://doi.org/10.1016/S2213-2600(17)30293-X.
[3] G.B.D.C.R.D. Collaborators, Prevalence and attributable health burden of chronic respiratory diseases, 1990-2017: a systematic analysis for the global burden of disease study 2017, Lancet Respir. Med. 8 (2020) 585–596, https://doi.org/10.1016/S2213-2600(20)30105-3.
[4] J. Chatkin, L. Correa, U. Santos, External environmental pollution as a risk factor for asthma, Clin. Rev. Allergy Immunol. 62 (2022) 72–89, https://doi.org/10.1007/s12016-020-08830-5.
[5] G.B.D.C.R.D. Collaborators, Global burden of chronic respiratory diseases and risk factors, 1990-2019: an update from the global burden of disease study 2019,

EClinicalMedicine 59 (2023) 101936, https://doi.org/10.1016/j.eclinm.2023.101936.
[6] N.C. Thomson, Challenges in the management of asthma associated with smoking-induced airway diseases, Expet Opin. Pharmacother. 19 (2018) 1565–1579, https://doi.org/10.1080/14656566.2018.1515912.
[7] K. Huang, et al., Prevalence, risk factors, and management of asthma in China: a national cross-sectional study, Lancet 394 (2019) 407–418, https://doi.org/10.1016/S0140-6736(19)31147-X.
[8] D. Mackay, S. Haw, J.G. Ayres, C. Fischbacher, J.P. Pell, Smoke-free legislation and hospitalizations for childhood asthma, N. Engl. J. Med. 363 (2010) 1139–1145, https://doi.org/10.1056/NEJMoa1002861.
[9] M. Oberg, M.S. Jaakkola, A. Woodward, A. Peruga, A. Pruss-Ustun, Worldwide burden of disease from exposure to second-hand smoke: a retrospective analysis of data from 192 countries, Lancet 377 (2011) 139–146, https://doi.org/10.1016/S0140-6736(10)61388-8.
[10] Y. Luo, S. Stent, Smoking's lasting effect on the immune system, Nature 626 (2024) 724–725, https://doi.org/10.1038/d41586-024-00232-3.
[11] J. Liu, et al., Interplay of il-33 and il-35 modulates th2/th17 responses in cigarette smoke exposure hdm-induced asthma, Inflammation 47 (2024) 173–190, https://doi.org/10.1007/s10753-023-01902-6.
[12] X. Yang, et al., A cpg-oligodeoxynucleotide suppresses th2/th17 inflammation by inhibiting il-33/st2 signaling in mice from a model of adoptive dendritic cell transfer of smoke-induced asthma, Int. J. Mol. Sci. 24 (2023) 3130, https://doi.org/10.3390/ijms24043130.
[13] I. D'Hulst A, K.Y. Vermaelen, G.G. Brusselle, G.F. Joos, R.A. Pauwels, Time course of cigarette smoke-induced pulmonary inflammation in mice, Eur. Respir. J. 26 (2005) 204–213, https://doi.org/10.1183/09031936.05.00095204.
[14] J. Zindel, P. Kubes, Damps, pamps, and lamps in immunity and sterile inflammation, Annu. Rev. Pathol. 15 (2020) 493–518, https://doi.org/10.1146/annurev-pathmechdis-012419-032847.
[15] V. Brinkmann, et al., Neutrophil extracellular traps kill bacteria, Science 303 (2004) 1532–1535, https://doi.org/10.1126/science.1092385.
[16] C. Xu, et al., Multifunctional boron-based 2d nanoplatforms ameliorate severe respiratory inflammation by targeting multiple inflammatory mediators, Adv. Sci. (2025) e2412626, https://doi.org/10.1002/advs.202412626.
[17] G. Sollberger, D.O. Tilley, A. Zychlinsky, Neutrophil extracellular traps: the biology of chromatin externalization, Dev. Cell 44 (2018) 542–553, https://doi.org/10.1016/j.devcel.2018.01.019.
[18] M. Dwyer, et al., Cystic fibrosis sputum DNA has netosis characteristics and neutrophil extracellular trap release is regulated by macrophage migration-inhibitory factor, J. Innate Immun. 6 (2014) 765–779, https://doi.org/10.1159/000363242.
[19] B. Curren, et al., Il-33-induced neutrophilic inflammation and netosis underlie rhinovirus-triggered exacerbations of asthma, Mucosal Immunol. 16 (2023) 671–684, https://doi.org/10.1016/j.mucimm.2023.07.002.
[20] C.H. Tsai, et al., Neutrophil extracellular trap production and ccl4l2 expression influence corticosteroid response in asthma, Sci. Transl. Med. 15 (2023) eadf3843, https://doi.org/10.1126/scitranslmed.adf3843.
[21] K. Hildenbrand, et al., Human interleukin-12alpha and ebi3 are cytokines with anti-inflammatory functions, Sci. Adv. 9 (2023) eadg6874, https://doi.org/10.1126/sciadv.adg6874.
[22] W. Peng, L. Wang, H. Zhang, Z. Zhang, X. Chen, Effects of recombinant il-35-bcg on treg/th17 cell imbalance and inflammatory response in asthmatic newborn mice induced by rsv, Inflammation 44 (2021) 2476–2485, https://doi.org/10.1007/s10753-021-01517-9.
[23] G.S. Whitehead, et al., Il-35 production by inducible costimulator (icos)-positive regulatory t cells reverses established il-17-dependent allergic airways disease, J. Allergy Clin. Immunol. 129 (2012) 207–215, https://doi.org/10.1016/j.jaci.2011.08.009, e201-205.
[24] J. Dong, et al., Amelioration of allergic airway inflammation in mice by regulatory il-35 through dampening inflammatory dendritic cells, Allergy 70 (2015) 921–932, https://doi.org/10.1111/all.12631.
[25] Z. Jin, et al., Neutrophil extracellular traps promote scar formation in post-epidural fibrosis, NPJ Regen. Med. 5 (2020) 19, https://doi.org/10.1038/s41536-020-00103-1.
[26] R. Al-Qazazi, et al., Macrophage-nlrp3 activation promotes right ventricle failure in pulmonary arterial hypertension, Am. J. Respir. Crit. Care Med. 206 (2022) 608–624, https://doi.org/10.1164/rccm.202110-2274OC.
[27] Y. Zhong, et al., The hdac10 instructs macrophage m2 program via deacetylation of stat3 and promotes allergic airway inflammation, Theranostics 13 (2023) 3568–3581, https://doi.org/10.7150/thno.82535.
[28] C. Li, et al., Fgf19-induced inflammatory caf promoted neutrophil extracellular trap formation in the liver metastasis of colorectal cancer, Adv. Sci. 10 (2023) e2302613, https://doi.org/10.1002/advs.202302613.
[29] D.F. Patel, et al., Neutrophils restrain allergic airway inflammation by limiting ilc2 function and monocyte-dendritic cell antigen presentation, Sci Immunol 4 (2019) eaax7006, https://doi.org/10.1126/sciimmunol.aax7006.
[30] H.R. Thiam, et al., Netosis proceeds by cytoskeleton and endomembrane disassembly and pad4-mediated chromatin decondensation and nuclear envelope rupture, Proc. Natl. Acad. Sci. U. S. A. 117 (2020) 7326–7337, https://doi.org/10.1073/pnas.1909546117.
[31] J. Zhao, et al., Nets promote inflammatory injury by activating cgas-sting pathway in acute lung injury, Int. J. Mol. Sci. 24 (2023) 5125, https://doi.org/10.3390/ijms24065125.
[32] Y. Wang, Y. Yu, W. Yu, X. Bian, L. Gong, Il-35 inhibits cell pyroptosis and attenuates cell injury in tnf-alpha-induced bronchial epithelial cells via p38 mapk signaling pathway, Bioengineered 13 (2022) 1758–1766, https://doi.org/10.1080/21655979.2021.2022266.
[33] R.H.L. Li, G. Ng, F. Tablin, Lipopolysaccharide-induced neutrophil extracellular trap formation in canine neutrophils is dependent on histone h3 citrullination by peptidylarginine deiminase, Vet. Immunol. Immunopathol. 193–194 (2017) 29–37, https://doi.org/10.1016/j.vetimm.2017.10.002.
[34] D. Wang, et al., Fluoride induces neutrophil extracellular traps and aggravates brain inflammation by disrupting neutrophil calcium homeostasis and causing ferroptosis, Environ. Pollut. 331 (2023) 121847, https://doi.org/10.1016/j.envpol.2023.121847.
[35] J. Liu, et al., Interleukin-33 modulates net formation via an autophagy-dependent manner to promote neutrophilic inflammation in cigarette smoke-exposure asthma, J. Hazard Mater. 487 (2025) 137257, https://doi.org/10.1016/j.jhazmat.2025.137257.
[36] S.J. Dixon, et al., Ferroptosis: an iron-dependent form of nonapoptotic cell death, Cell 149 (2012) 1060–1072, https://doi.org/10.1016/j.cell.2012.03.042.
[37] X.Y. He, et al., Chronic stress increases metastasis via neutrophil-mediated changes to the microenvironment, Cancer Cell 42 (2024) 474–486, https://doi.org/10.1016/j.ccell.2024.01.013, e412.
[38] H. Zhang, et al., Neutrophil extracellular traps mediate m(6)a modification and regulates sepsis-associated acute lung injury by activating ferroptosis in alveolar epithelial cells, Int. J. Biol. Sci. 18 (2022) 3337–3357, https://doi.org/10.7150/ijbs.69141.
[39] Z. Zhang, Q. Zhu, S. Wang, C. Shi, Epigallocatechin-3-gallate inhibits the formation of neutrophil extracellular traps and suppresses the migration and invasion of colon cancer cells by regulating stat3/cxcl8 pathway, Mol. Cell. Biochem. 478 (2023) 887–898, https://doi.org/10.1007/s11010-022-04550-w.
[40] M. Zhu, et al., Stat3 signaling promotes cardiac injury by upregulating ncoa4-mediated ferritinophagy and ferroptosis in high-fat-diet fed mice, Free Radic. Biol. Med. 201 (2023) 111–125, https://doi.org/10.1016/j.freeradbiomed.2023.03.003.
[41] S. Lin, J. Yan, W. Wang, L. Luo, Stat3-mediated ferroptosis is involved in sepsis-associated acute respiratory distress syndrome, Inflammation 47 (2024) 1204–1219, https://doi.org/10.1007/s10753-024-01970-2.
[42] L.W. Collison, et al., The composition and signaling of the il-35 receptor are unconventional, Nat. Immunol. 13 (2012) 290–299, https://doi.org/10.1038/ni.2227.
[43] A. Huang, et al., Il-35 stabilizes treg phenotype to protect cardiac allografts in mice, Transplantation 108 (2024) 161–174, https://doi.org/10.1097/TP.0000000000004707.
[44] X. Zhou, et al., Interleukin 35 ameliorates myocardial ischemia-reperfusion injury by activating the gp130-stat3 axis, FASEB J. 34 (2020) 3224–3238, https://doi.org/10.1096/fj.201901718RR.
[45] Z. Cai, et al., A novel potential target of il-35-regulated jak/stat signaling pathway in lupus nephritis, Clin. Transl. Med. 11 (2021) e309, https://doi.org/10.1002/ctm2.309.
[46] M. Baastrup Soendergaard, et al., Tobacco exposure and efficacy of biologic therapy in patients with severe asthma: a nationwide study from the Danish severe asthma register, J. Allergy Clin. Immunol. Pract. 12 (2024) 146–155, https://doi.org/10.1016/j.jaip.2023.10.012, e145.
[47] L.S. Flor, et al., Health effects associated with exposure to secondhand smoke: a burden of proof study, Nat. Med. 30 (2024) 149–167, https://doi.org/10.1038/s41591-023-02743-4.
[48] N.C. Thomson, R. Polosa, D.D. Sin, Cigarette smoking and asthma, J. Allergy Clin. Immunol. Pract. 10 (2022) 2783–2797, https://doi.org/10.1016/j.jaip.2022.04.034.
[49] A.E. Sprio, et al., The influence of smoking on asthma in the real-life, Respir. Med. 170 (2020) 106066, https://doi.org/10.1016/j.rmed.2020.106066.
[50] M.G. Belvisi, et al., Modelling the asthma phenotype: impact of cigarette smoke exposure, Respir. Res. 19 (2018) 89, https://doi.org/10.1186/s12931-018-0799-7.
[51] X. He, et al., Pm2.5 aggravates nqo1-induced mucus hyper-secretion through release of neutrophil extracellular traps in an asthma model, Ecotoxicol. Environ. Saf. 218 (2021) 112272, https://doi.org/10.1016/j.ecoenv.2021.112272.
[52] G.S. Whitehead, et al., A neutrophil/tgf-beta axis limits the pathogenicity of allergen-specific cd4+ t cells, JCI Insight 7 (2022) e150251, https://doi.org/10.1172/jci.insight.150251.
[53] T.C. Brembach, R. Sabat, K. Witte, T. Schwerdtle, K. Wolk, Molecular and functional changes in neutrophilic granulocytes induced by nicotine: a systematic review and critical evaluation, Front. Immunol. 14 (2023) 1281685, https://doi.org/10.3389/fimmu.2023.1281685.
[54] B.D. Levy, et al., Multi-pronged inhibition of airway hyper-responsiveness and inflammation by lipoxin a(4), Nat. Med. 8 (2002) 1018–1023, https://doi.org/10.1038/nm748.
[55] C. Barnig, et al., Lipoxin a4 regulates natural killer cell and type 2 innate lymphoid cell activation in asthma, Sci. Transl. Med. 5 (2013) 174ra126, https://doi.org/10.1126/scitranslmed.3004812.
[56] M.E. Deerhake, E.D. Cardakli, M.L. Shinohara, Dectin-1 signaling in neutrophils up-regulates pd-l1 and triggers ros-mediated suppression of cd4(+) t cells, J. Leukoc. Biol. 112 (2022) 1413–1425, https://doi.org/10.1002/JLB.3A0322-152RR.
[57] A.S. Wilson, et al., Neutrophil extracellular traps and their histones promote th17 cell differentiation directly via tlr2, Nat. Commun. 13 (2022) 528, https://doi.org/10.1038/s41467-022-28172-4.
[58] T.S. Kim, et al., Neutrophil extracellular traps and extracellular histones potentiate il-17 inflammation in periodontitis, J. Exp. Med. 220 (2023) e20221751, https://doi.org/10.1084/jem.20221751.

[59] E.A. Cafferata, et al., Interleukin-35 inhibits alveolar bone resorption by modulating the th17/treg imbalance during periodontitis, J. Clin. Periodontol. 47 (2020) 676–688, https://doi.org/10.1111/jcpe.13282.
[60] X.H. Bao, F. Gao, S.S. Athari, H. Wang, Immunomodulatory effect of il-35 gene-transfected mesenchymal stem cells on allergic asthma, Fundam. Clin. Pharmacol. 37 (2023) 116–124, https://doi.org/10.1111/fcp.12823.
[61] C. Chu, et al., Neutrophil extracellular traps drive intestinal microvascular endothelial ferroptosis by impairing fundc1-dependent mitophagy, Redox Biol. 67 (2023) 102906, https://doi.org/10.1016/j.redox.2023.102906.
[62] P. Zhao, et al., Neutrophil extracellular traps mediate cardiomyocyte ferroptosis via the hippo-yap pathway to exacerbate doxorubicin-induced cardiotoxicity, Cell. Mol. Life Sci. 81 (2024) 122, https://doi.org/10.1007/s00018-024-05169-4.
[63] D. Chen, G. Zheng, Q. Yang, L. Luo, J. Shen, Il-35 subunit ebi3 alleviates bleomycin-induced pulmonary fibrosis via suppressing DNA enrichment of stat3, Respir. Res. 22 (2021) 280, https://doi.org/10.1186/s12931-021-01858-x.
[64] X. Yong, et al., Cdkn2a inhibited ferroptosis through activating jak2/stat3 pathway to modulate cisplatin resistance in cervical squamous cell carcinoma, Anti Cancer Drugs 35 (2024) 698–708, https://doi.org/10.1097/CAD.0000000000001620.
[65] W. Zhang, et al., Thiostrepton induces ferroptosis in pancreatic cancer cells through stat3/gpx4 signalling, Cell Death Dis. 13 (2022) 630, https://doi.org/10.1038/s41419-022-05082-3.
[66] J.Q. Lai, et al., Baicalein triggers ferroptosis in colorectal cancer cells via blocking the jak2/stat3/gpx4 axis, Acta Pharmacol. Sin. 45 (2024) 1715–1726, https://doi.org/10.1038/s41401-024-01258-z.
[67] Y. Li, et al., Neutrophils and il17a mediate flagellar hook protein flge-induced mouse acute lung inflammation, Cell. Microbiol. 21 (2019) e12975, https://doi.org/10.1111/cmi.12975.
[68] R.X. Wang, et al., Interleukin-35 induces regulatory b cells that suppress autoimmune disease, Nat. Med. 20 (2014) 633–641, https://doi.org/10.1038/nm.3554.
[69] M. Maddaloni, I. Kochetkova, C. Hoffman, D.W. Pascual, Delivery of il-35 by lactococcus lactis ameliorates collagen-induced arthritis in mice, Front. Immunol. 9 (2018) 2691, https://doi.org/10.3389/fimmu.2018.02691.
[70] S. Hu, et al., The role of il-35 in the pathophysiological processes of liver disease, Front. Pharmacol. 11 (2020) 569575, https://doi.org/10.3389/fphar.2020.569575.
[71] C. Ye, H. Yano, C.J. Workman, D.A.A. Vignali, Interleukin-35: structure, function and its impact on immune-related diseases, J. Interferon Cytokine Res. 41 (2021) 391–406, https://doi.org/10.1089/jir.2021.0147.
[72] N.T. Fiore, J.P. Hayes, S.I. Williams, G. Moalem-Taylor, Interleukin-35 alleviates neuropathic pain and induces an anti-inflammatory shift in spinal microglia in nerve-injured male mice, Brain Behav. Immun. 122 (2024) 287–300, https://doi.org/10.1016/j.bbi.2024.07.043.